AD-A044 242 CALIFORNIA UNIV LOS ANGELES SCHOOL OF ENGINEERING A--ETC F/G 20/11
INTERNAL STRESSES DUE TO AN OBLATE SPHEROIDAL INCLUSION; MISFIT--ETC(U)
AUG 77 M SHIBATA, K ONO N00014-75-C-0889

UNCLASSIFIED TR-4 NL

| OF |
ADA
044242

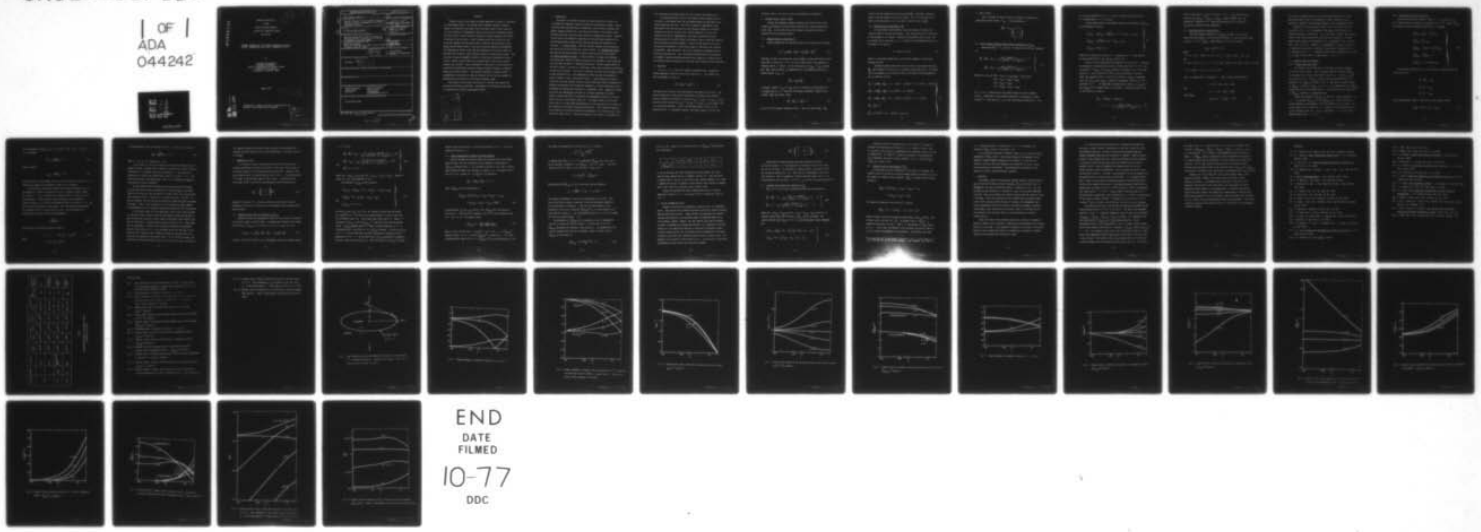

END
DATE
FILMED
10-77
DDC

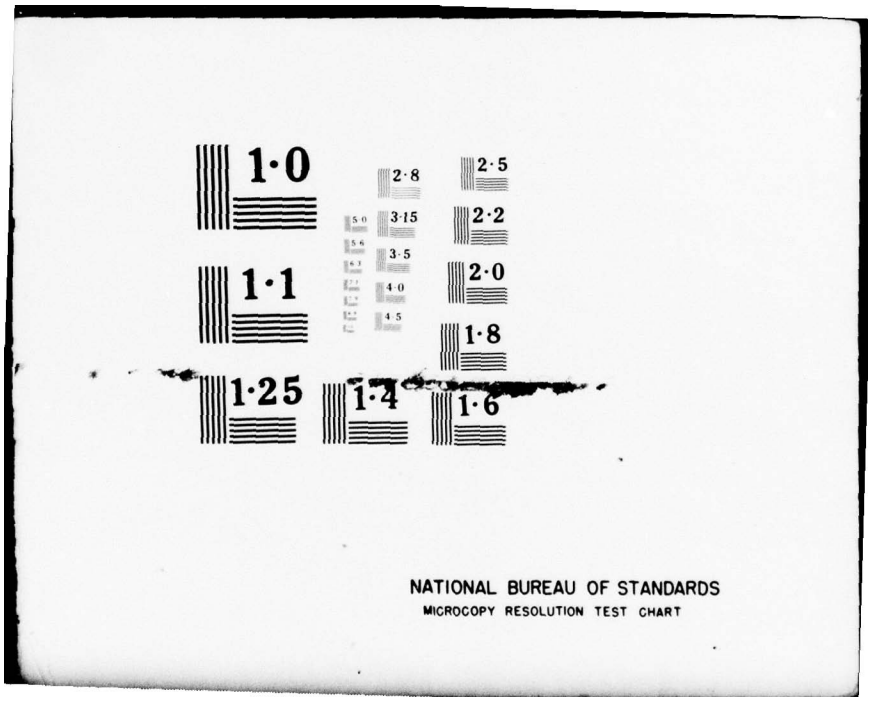
1·0
1·1
1·25
1·4
1·6
1·8
2·0
2·2
2·5
2·8
3·15
3·5
4·0
4·5
5·0
5·6
6·3
NATIONAL BUREAU OF STANDARDS
MICROCOPY RESOLUTION TEST CHART

(12)

Technical Report No. 4

to the

Office of Naval Research

Contract No. N00014-75-C-0889

NR 031-781

INTERNAL STRESSES DUE TO AN OBLATE SPHEROIDAL INCLUSION; MISFIT, INHOMOGENEITY AND PLASTIC DEFORMATION EFFECTS

by

M. Shibata and Kanji Ono
MATERIALS DEPARTMENT
School of Engineering and Applied Science
University of California
Los Angeles, California 90024

August 1977

SECURITY CLASSIFICATION OF THIS PAGE *(When Data Entered)*

REPORT DOCUMENTATION PAGE

READ INSTRUCTIONS BEFORE COMPLETING FORM

1. REPORT NUMBER: ONR Technical Report # 4
2. GOVT ACCESSION NO.:
3. RECIPIENT'S CATALOG NUMBER: (9)

4. TITLE *(and Subtitle)*: (6) Internal Stresses Due to an Oblate Spheroidal Inclusion; Misfit, Inhomogeneity and Plastic Deformation Effects.

5. TYPE OF REPORT & PERIOD COVERED: Technical Report

6. PERFORMING ORG. REPORT NUMBER:

7. AUTHOR(s): (10) M. Shibata and Kanji Ono

8. CONTRACT OR GRANT NUMBER(s): (15) N00014-75-C-0889
NR 031-871

9. PERFORMING ORGANIZATION NAME AND ADDRESS:
Materials Department, School of Engineering
6531-Boelter Hall, University of California
Los Angeles, California 90024

10. PROGRAM ELEMENT, PROJECT, TASK AREA & WORK UNIT NUMBERS: (11)

11. CONTROLLING OFFICE NAME AND ADDRESS:
Metallurgy Program
Office of Naval Research, 800 N. Quincy Street
Arlington, Virginia 22217

12. REPORT DATE: August 1977

13. NUMBER OF PAGES: 40

14. MONITORING AGENCY NAME & ADDRESS *(if different from Controlling Office)*: (12) 44p.

15. SECURITY CLASS. *(of this report)*: unclassified

15a. DECLASSIFICATION/DOWNGRADING SCHEDULE:

16. DISTRIBUTION STATEMENT *(of this Report)*
Unlimited (17) TR-4

17. DISTRIBUTION STATEMENT *(of the abstract entered in Block 20, if different from Report)*

18. SUPPLEMENTARY NOTES

19. KEY WORDS *(Continue on reverse side if necessary and identify by block number)*

Internal Stresses
Strain Energy
Inclusion
Elasticity Theory
Misfit Strain
Inhomogeneity
Non-Deformable Particle

20. ABSTRACT *(Continue on reverse side if necessary and identify by block number)*

See Following Page

DD FORM 1 JAN 73 1473 EDITION OF 1 NOV 65 IS OBSOLETE
S/N 0102 LF 014 6601

SECURITY CLASSIFICATION OF THIS PAGE *(When Data Entered)*

404637

ABSTRACT

Internal stress in and around an oblate spheroidal inclusion is evaluated by using Eshelby theory. We consider three different sources of internal stress as a function of the aspect ratio and elastic moduli ratio; these are (1) misfit effect (2) inhomogeneity effect and (3) plastic deformation effect. The misfit effect arises from the difference of thermal expansion coefficients of the matrix and inclusion. Normal stresses within the inclusion (or the principal stresses), maximum shear stress inside the inclusion, total strain energy and the normal stress at the matrix-inclusion boundary are determined. The inhomogeneity effect arises from the difference of the elastic moduli of the matrix and inclusion, which perturbs otherwise uniform applied stress. The direction of applied stress is parallel to the axis of revolution of the inclusion. Normal stresses within the inclusion and at the matrix-inclusion boundary are obtained. Plastic deformation of the matrix in the presence of a plastically non-deformable inclusion produces internal stresses, as shown by Ashby and by Tanaka and Mori. The approach developed by Tanaka and Mori is extended here to evaluate the internal stresses for the inclusion geometries appropriate to the analysis of technically important cases.

The results of the present calculations in limiting cases agree with previously published calculations. Implications of the results are dicussed in connection with several experimental studies.

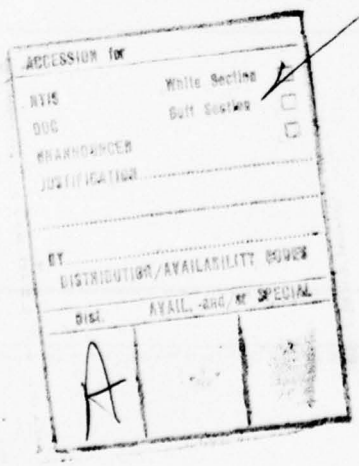

1. INTRODUCTION

Inclusions in a material are known to exert significant influence on its mechanical properties, especially ductility and fracture strength. Typical inclusions have different physical properties, such as elastic constants and thermal expansion coefficient, from those of the matrix, and internal stress develops around the inclusions upon stressing or temperature changes. Important in the study of the mechanical properties of inclusion bearing materials are the following three internal stress problems caused by the presence of an inclusion: (1) Misfit Effect: How high internal stresses can be produced in and around the inclusion which has a misfit strain? (2) Inhomogeneity Effect: How does the inclusion perturb an external stress applied to the material? (3) Plastic Deformation Effect: If the inclusion is assumed to be deformed only elastically, how much internal stresses can be developed in and around the inclusion when the matrix is deformed plastically? The most common example of the misfit effect is one due to a difference in the thermal expansion coefficients of matrix and inclusion. The case of a spherical inclusion was thoroughly studied by Mott and Nabarro [1]. The inhomogeneity effect has been investigated in order to obtain a stress concentration factor. A penny-shaped cavity and an elliptical hole were treated initially and have been most widely considered [2,3]. Sadowsky and Sternberg [4] extended the treatment to a prolate spheroidal cavity, and Nauber [5] obtained the solution for a spheroidal cavity. Edwards [6] solved the misfit and inhomogeneity problems for a prolate spheroidal inclusion. Recently, Mirandy and Paul [7] evaluated the inhomogeneity effect for an ellipsoidal cavity by using Eshelby theory [8]. The Eshelby theory of the elastic strain field in a constrained transformation also was the basis of the Tanaka and Mori analysis of the plastic deformation effect [9]. Their method was applied to the analysis of inclusion fracture and decohesion in the limiting case of the inclusion's shape [10,11]. Additional studies of this effect as it pertains to

work hardening of multiphase materials have also been published [12,13].

In surveying previous works on the internal stress problems due to an inclusion, it has become clear that no detailed study has been made for an oblate spheroidal inclusion. Yet, this is central in importance in the applications involving the ductility and fracture strength of a material. Therefore, we wish to evaluate for an oblate spheroidal inclusion with respect to the misfit, inhomogeneity, and plastic deformation effects. Eshelby theory [8] is used to obtain the internal stress inside the inclusion and at the matrix-inclusion boundary. Effects of the aspect ratio of the inclusion and differences in the elastic moduli of the matrix and inclusion are examined. When applicable, the results obtained are compared with the previously published one. Also described are applications to the analysis of thermally induced dislocation-punching from a spherical inclusion, and to the internal stress evaluation of a structural steel containing MnS inclusions.

2. INCLUSION

Let X_i (i = 1, 2, and 3) be Cartesian coordinate axes. Consider an oblate spheroidal inclusion at the origin (see Fig. 1). Its volume is V_I, and its boundary is given as,

$$(x_1^2 + x_2^2)/a^2 + x_3^2/c^2 = 1 \ . \qquad (1)$$

The shape of an inclusion can be described by the aspect ratio k(=c/a). The elastic properties of the inclusion and matrix are assumed to be isotropic. Elastic stiffness of the matrix is given by $C_{ijk\ell} = \lambda\delta_{ij}\delta_{k\ell} + \mu(\delta_{ik}\delta_{j\ell} + \delta_{jk}\delta_{i\ell})$ and that of the inclusion by $C^*_{ijk\ell} = \lambda^*\delta_{ij}\delta_{k\ell} + \mu^*(\delta_{ik}\delta_{j\ell} + \delta_{jk}\delta_{i\ell})$ where λ and λ^* are the Lamé constants, μ and μ^* are the shear moduli, and δ_{ij} is the Kronecker delta. In subsequent sections, the Young's modulus (E or E*) and

Poisson's ratio (ν or ν^*) will also be used because of convenience.

3. INTERNAL STRESS; ESHELBY THEORY

Eshelby [8] developed a method to analyze the elastic field in and around an ellipsoidal inclusion, within which exists a uniform stress-free strain, $\mathbf{e}_{ij}^{T*}$. In this study we use this theory to evaluate the internal stresses of the inclusion and matrix.

3-1. Internal Stress of Inclusion, σ_{ij}^{I}

Eshelby showed that the internal stress of an inclusion can be written as,

$$\sigma_{ij}^{I} = C_{ijk\ell}(\mathbf{e}_{k\ell}^{C} - \mathbf{e}_{k\ell}^{T}) = C_{ijk\ell}^{*}(\mathbf{e}_{k\ell}^{C} - \mathbf{e}_{k\ell}^{T*}) \tag{2}$$

where $\mathbf{e}_{k\ell}^{C}$ is total (or constraint) strain and $\mathbf{e}_{k\ell}^{T}$ is stress-free strain of the equivalent inclusion [8]. In Eq. (2) and in what follows, the summation of repeated indices is implied. In the limiting case of $C_{ijk\ell} = C_{ijk\ell}^{*}$, we have $\mathbf{e}_{k\ell}^{T} = \mathbf{e}_{k\ell}^{T*}$, hence we obtain σ_{ij}^{I} immediately for a given $\mathbf{e}_{k\ell}^{T*}$ with the use of Eshelby tensor, $S_{ijk\ell}$, as

$$\mathbf{e}_{k\ell}^{C} = S_{k\ell mn}\, \mathbf{e}_{mn}^{T} \,. \tag{3}$$

In general, however, $C_{ijk\ell} \neq C_{ijk\ell}^{*}$, and it is necessary to obtain $\mathbf{e}_{ij}^{T}$ for a given $\mathbf{e}_{ij}^{T*}$ using Eq. (2). When the off-diagonal components of $\mathbf{e}_{ij}^{T*}$ are zero and $\mathbf{e}_{11}^{T*} = \mathbf{e}_{22}^{T*}$, $\mathbf{e}_{ij}^{T}$ becomes simply

$$\mathbf{e}_{11}^{T} = \mathbf{e}_{22}^{T} = x, \; \mathbf{e}_{33}^{T} = z, \tag{4}$$

and all the off-diagonal components vanish. Here, the equality $\mathbf{e}_{11}^{T} = \mathbf{e}_{22}^{T}$

results from the symmetry of the inclusion and ε_{ij}^{T*}. Therefore, remaining tasks in the calculation of σ_{ij}^{I} are to obtain (x,z) as a function of the ratios of elastic moduli; i.e., μ^*/μ and ν^*/ν and k as well as ε_{ij}^{T*}.

3-2. Internal Stress of the Matrix, σ_{ij}^{M}

As the distance from the matrix-inclusion boundary increases, the internal stress of the matrix decreases. Thus, the stress state of the matrix at the boundary is of interest. Because of the symmetry about x_3 axis, let us consider σ_{ij}^{M} on the plane, $x_2 = 0$. At point D on the boundary (see Fig. 1), the normal $\bar{n}$, is given by

$$\bar{n} = (\cos\theta,\ 0,\ \sin\theta), \tag{5}$$

where θ is the angle between the x_3 axis and the tangential line passing through the point.

Eshelby [8] deduced the total strain of matrix just outside inclusion, ε_{ij}^{M}, which remains to be elastic, as a function of ε_{ij}^{c}, ε_{ij}^{T} and $\bar{n}$. It follows that the components of the internal stress of the matrix at the boundary on the x_2 plane are given by

$$\left.\begin{aligned}
\sigma_{11}^{M} &= \mu\{2(3\varepsilon_{11}^{c} + \varepsilon_{33}^{c}) - (2 + 7\cos^2\theta - 3\cos^4\theta)x - (2 - 3\cos^2\theta + 3\cos^4\theta)z\} \\
\sigma_{22}^{M} &= \mu\{2(3\varepsilon_{11}^{c} + \varepsilon_{33}^{c}) - (2 + \cos^2\theta)x - (2 - \cos^2\theta)z\} \\
\sigma_{33}^{M} &= \mu\{4(\varepsilon_{11}^{c} + \varepsilon_{33}^{c}) - (4 - 4\cos^2\theta + 3\cos^4\theta)x - (4 - 3\cos^4\theta)z\} \\
\sigma_{12}^{M} &= \sigma_{23}^{M} = 0 \\
\sigma_{13}^{M} &= \mu\{(3\cos^2\theta - 4)x - (3\cos^2\theta)z\}\sin\theta\cos\theta\ .
\end{aligned}\right\} \tag{6}$$

4. MISFIT EFFECT

Let us consider the case in which an inclusion is subjected to a hydro-static misfit strain, $\varepsilon^T\delta_{ij}$. It can be written as

$$\mathbf{e}_{ij}^{T*} = \varepsilon^T\delta_{ij} = \begin{pmatrix} \varepsilon^T & 0 & 0 \\ 0 & \varepsilon^T & 0 \\ 0 & 0 & \varepsilon^T \end{pmatrix}.$$

4-1. Misfit Induced Internal Stress Within an Inclusion, $(\sigma_{ij}^I)_{mis}$

Substituting $\mathbf{e}_{ij}^{T*} = \varepsilon^T\delta_{ij}$ into Eq. (2), $\mathbf{e}_{ij}^T$ due to misfit are obtained as,

$$\left.\begin{aligned} \mathbf{e}_{11}^T = \mathbf{e}_{22}^T = x_{mis} &= \frac{m\{(1-m)h(k)+1\}}{\{(1-m)^2 f(k) - (1-m)g(k)+1\}} \cdot \varepsilon^T \\ \mathbf{e}_{33}^T = z_{mis} &= \frac{m\{(1-m)\ell(k)+1\}}{\{(1-m)^2 f(k) - (1-m)g(k)+1\}} \cdot \varepsilon^T \end{aligned}\right\} \quad (7)$$

where m is μ^*/μ, and $f(k) = (S_{1111} + S_{1122})S_{3333} - 2S_{1133}S_{3311}$,

$$g(k) = S_{1111} + S_{1122} + S_{3333},$$

$$h(k) = S_{1133} - S_{3333},$$

$$\ell(k) = 2S_{3311} - S_{1111} - S_{1122}.$$

For k = 0 or 1, these terms of the Eshelby tensor are given elsewhere [13,14]. Integration of the original expressions is necessary for other values of k. The values of f, g, h, and ℓ have been evaluated for k = 0.01

to 1 and are presented in Fig. 2. In order to simplify the calculations, it is assumed that $\nu = \nu^* = 1/3$ holds.

From the above results, the internal stress of the inclusion, $(\sigma^I_{ij})_{mis}$, can be obtained as follows:

$$\left.\begin{aligned}
(\sigma^I_{11})_{mis} &= (\sigma^I_{22})_{mis} = \frac{3E^*}{4(1-m)} \cdot \{-4\varepsilon^T + (3x_{mis} + z_{mis})\} \\
(\sigma^I_{33})_{mis} &= \frac{3E^*}{2(1-m)} \cdot \{-2\varepsilon^T + (x_{mis} + z_{mis})\} \\
(\sigma^I_{ij})_{mis} &= 0 \text{ when } i \neq j \ .
\end{aligned}\right\} \quad (8)$$

Note that no singularity exists at $m = 1$, because the $(1 - m)$ term factors out upon substitution of x_{mis} and z_{mis} into Eq. (8).

Results of the calculations are presented in Figures 3 and 4. Stresses are expressed in dimensionaless forms by dividing them by $E^*\varepsilon^T$ or $\mu^*\varepsilon^T$. The variations of $(\sigma^I_{11})_{mis}$ and $(\sigma^I_{33})_{mis}$ against k are shown in Fig. 3 for three values of m. One can see that, as the inclusion approaches a thin disc shape, the component normal to the plane of the disc, $(\sigma^I_{33})_{mis}$, approaches zero, and $(\sigma^I_{11})_{mis}$ and $(\sigma^I_{22})_{mis}$ approach an asympototic value of $-1.5\ \varepsilon^T E^*$ regardless of m. The magnitude of dimensionless stresses, $(\sigma^I_{11})_{mis}/E^*\varepsilon^T$ and $(\sigma^I_{33})_{mis}/E^*\varepsilon^T$, becomes larger as m decreases. The maximum shear stress in the inclusion is given by

$$\begin{aligned}
\tau^I_{mis} &= \{(\sigma^I_{33})_{mis} - (\sigma^I_{11})_{mis}\}/2 \\
&= \mu^* \cdot \varepsilon^T \cdot \frac{m\{\ell(k) - h(k)\}}{\{(1-m)^2 f(k) - (1-m)g(k) + 1\}} \ . \qquad (9)
\end{aligned}$$

Figure 4 show plots of $\tau^I_{mis}/\mu^*\varepsilon^T$ against k. At k = 1, τ^I_{mis} vanishes due to the equality $(\sigma^I_{11})_{mis} = (\sigma^I_{22})_{mis} = (\sigma^I_{33})_{mis}$. When k becomes zero, τ^I_{mis} reaches $2\mu^*\varepsilon^T$ regardless of m. Note that the effect of m is smaller on τ^I_{mis} than on the normal stress components.

4-2. Strain Energy Due to Misfit Strain

Once the diagonal components of $(\sigma^I_{ij})_{mis}$ are known, it is easy to obtain the strain energy E_s due to the misfit effect. E_s can be written simply as, $E_s/V_I = -0.5\,\varepsilon^T(\sigma^I_{kk})_{mis}$. When neither μ^*/μ nor ν^*/ν is unity,

$$E_s/V_I = \mu^*(\varepsilon^T)^2 \cdot P/Q$$

where

$$P = (1+\nu)(1+\nu^*)[3(1-\nu) + 3(1-m)(1-\nu)\{f(k) - g(k)\} - m(1+\nu)]$$

and

$$Q = [(1-m)(1+\nu)(1-\nu)(1-2\nu^*)\{f(k) - g(k)\} - m(1-m)(1-2\nu)(1+\nu^*) f(k)$$

$$+ (1+\nu)\{m(\nu^* - \nu) + (1-\nu)(1-2\nu^*)\}].$$

At k = 0, we have f(0) = 0 and g(0) = 1. Thus, P and Q are simplified as

$$P = 2(1+\nu)(1+\nu^*)(1-2\nu)m$$

and

$$Q = (1+\nu)(1-\nu^*)(1-2\nu)m,$$

which yield

$$E_s/V_I = 2\mu^* \cdot \frac{1+\nu^*}{1-\nu^*} \cdot (\varepsilon^T)^2. \qquad (10)$$

This result is apparently equal to that derived by Robinson [15], except that the Poisson's ratio in the numerator is that of the matrix in his expression. However, this discrepancy appears to be a typographical error.

Regardless of the aspect ratio, when μ^* and μ are equal, E_s can be given by Eq. (10). E_s is independent of the shape of the inclusion, as originally deduced by Eshelby [8]. In his derivation, however, the Poisson's ratios of the inclusion and matrix were taken to be identical. For more general cases, aspect ratio dependence of E_s is presented in Fig. 5, taking both ν and ν^* to be 1/3. Whereas E_s is independent of k when m is unity, it is interesting to note that a spherical inclusion has a minimum E_s for $m > 1$ or a maximum E_s for $m < 1$. In agreement with findings of Barnett et al. [16], E_s is larger in discs than in a sphere when $m > 1$ (or $\mu^* > \mu$).

4-3. Internal Stress of the Matrix

4-3-1. Equator and Polar Points

The internal stress of the matrix at the matrix-inclusion boundary varies from point to point. Here, we present numerical values of $(\sigma^M_{33})_{mis}$ at an equator point A and a polar point B (see Fig. 1). By using x_{mis} and z_{mis} given in Eq. (7), $(\sigma^M_{ij})_{mis}$ at A and B can be obtained from Eq. (6). The results for $(\sigma^M_{33})_{mis}$ are shown in Fig. 6. Note that at the polar point B, $(\sigma^M_{33})_{mis}$ is equal to $(\sigma^I_{33})_{mis}$ (cf. Fig. 2). As k becomes smaller, $(\sigma^M_{33})_{mis}$ depends more on m at the equator point A. At the polar point B, effect of m on $(\sigma^M_{33})_{mis}$ increases as k approaches unity.

Edwards [6] calculated $(\sigma^M_{ij})_{mis}$ at A and B for prolate spheroids; i.e., $k \geq 1$. He obtained $(\sigma^M_{11})_{mis}$ at A and $(\sigma^M_{33})_{mis}$ at B. These are both the normal component at the boundary, and can be obtained from σ^I_{ij} easily. Our results agree with his results at $k = 1$, except for small discrepancies due to the different values of ν. In our calculations, $\nu = \nu^* = 1/3$ is used whereas Edwards took $\nu = \nu^* = 0.3$.

4-3-2. Maximum Shear Stress of the Matrix

When an inclusion takes spherical shape, (k = 1), x_{mis} and z_{mis} in Eq. (7) become identical because of an equality h(1) = ℓ(1). Hence, $(\sigma^M_{ij})_{mis}$ at the matrix-inclusion boundary on the plane $x_2 = 0$ becomes

$$\left.\begin{aligned}
(\sigma^M_{11})_{mis} &= \frac{4}{3}\cdot\mu(1 - \cos^2\theta)x_{mis} \\
(\sigma^M_{22})_{mis} &= \frac{4}{3}\cdot\mu\, x_{mis} \\
(\sigma^M_{33})_{mis} &= -\frac{4}{3}\cdot\mu(2 - 3\cos^2\theta)x_{mis} \\
(\sigma^M_{12})_{mis} &= (\sigma^M_{23})_{mis} = 0 \\
(\sigma^M_{13})_{mis} &= -4\mu \sin\theta\cos\theta\, x_{mis}\,.
\end{aligned}\right\} \qquad (11)$$

The principal stresses of Eq. (11) are given by a rotation about the x_2 axis by $(-\theta)$ as

$$\sigma^M_1 = \frac{-10}{3}\cdot\mu\, x_{mis}$$

$$\sigma^M_2 = \frac{4}{3}\cdot\mu\, x_{mis}$$

$$\sigma^M_3 = \frac{2}{3}\cdot\mu\, x_{mis}$$

and the maximum shear stress of the matrix at the boundary becomes

$$|\tau^M_{max}| = \frac{1}{2}\,|\sigma^M_1 - \sigma^M_3| = 2\mu|x_{mis}|\,. \qquad (12)$$

This corresponds to $(\sigma^M_{13})_{mis}$ in Eq. (11) with $\theta = 45°$. At $k = 1$, x_{mis} in Eq. (7) becomes

$$x_{mis} = \frac{3m}{(2m + 1)} \cdot \varepsilon^T, \tag{13}$$

hence, we obtain

$$|\tau_{max}| = \frac{6m}{1 + 2m} \mu \cdot |\varepsilon^T|. \tag{14}$$

The factor $6m/(1 + 2m)$ increases from 0 to 2 for a change in m from 0 to 1. It gradually increases to the asymptotic value of 3 as m diverges.

This particular problem was treated first by Mott and Nabarro [1] via the method of "a centre of dilatation" [17,18]. Suppose an elastic sphere of a radius $(1 + \varepsilon^T)a_0$ is forced into a spherical hole of a radius a_0 in an infinite matrix. After removing surface tractions, which squeeze the sphere to radius a_0, its equilibrium boundary relaxes to a radius $a = (1 + \varepsilon)a_0$. Let K* be the bulk modulus of the sphere. Also "the effective bulk modulus for expanding a hole" is taken to be $4\mu/3$ [19]. From the balance of a radial stress, we have as the first approximation,

$$\varepsilon = \frac{3K^*}{3K^* + 4\mu} \cdot \varepsilon^T. \tag{15}$$

The stress at X_i outside the sphere is given by

$$\sigma_{ij} = 2\mu \cdot \varepsilon \cdot a^3(\delta_{ij}/r^3 - 3X_iX_j/r^5) \tag{16}$$

where

$$r = (X_1^2 + X_2^2 + X_3^2)^{1/2}.$$

The maximum shear stress is obtained at $(a/\sqrt{2}\ ,\ 0,\ a/\sqrt{2}\ )$, and is given by

$$\tau^{M}_{max} = \frac{-9K^*}{3K^* + 4\mu} \cdot \mu \cdot \varepsilon^{T} \ . \qquad (17)$$

When $\nu^* = 1/3$, Eq. (17) reduces to Eq. (14).

Let us apply Eq. (14) to the analysis of dislocation generation due to thermal stresses. Consider that a spherical inclusion has a thermal expansion coefficient, α^*, different from that of the matrix, α. The inclusion is subjected to a stress-free transformation strain $\varepsilon^{T}\delta_{ij}$ with $\varepsilon^{T} = (\alpha^* - \alpha)\Delta T$ after cooling from a high temperature. Here, ΔT is a temperature change in the absence of plastic relaxation.

We have examined three different cases in which electron microscopy study was made and the physical properties to calculate τ^{M}_{max} are available. These are (1) $A\ell_2O_3$ and ZrO_2 inclusions in Fe matrix [20], (2) a borosilicate glass inclusion in $AgC\ell$ [21] and (3) a carbide inclusion in Mo [22]. In the last example, the inclusion was not positively identified, but was assumed to be Mo_2C. Table I lists the results of our calculation of τ^{M}_{max} together with experimental data and comments regarding the observations of dislocations.

If dislocation loops are to be generated at the critical shear strength in a perfect crystal of about $\mu/30$ [23], the present results indicate that a borosilicate glass inclusion in $AgC\ell$ produces dislocation loops around it and that no dislocation is produced around an $A\ell_2O_3$ inclusion in Fe. These agree with the experiments. However, some irregular dislocations were observed around a ZrO_2 inclusion in Fe. The calculated result show that τ^{M}_{max} is much less than $\mu/30$, suggesting that irregular dislocations observed around ZrO_2 inclusions are produced by non-thermal stress. As for the third example, the calculation indicates that Mo_2C inclusion is not likely to create dislocations.

This suggests either that prismatic loops observed in the experiment has resulted from the interaction with glide dislocations, or that the inclusion is not Mo_2C.

5. INHOMOGENEITY EFFECT

If a perfectly fitting inclusion with no misfit strain has elastic constants differieng form those of the matrix, the elastic field caused by an external source will be distrubed around the inclusion. Suppose an uniaxial external stress is applied along X_3 axis in Fig. 1. The applied stress σ^A is equal to σ^A_{33} and other terms of σ^A_{ij} is zero. It produces elastic strain, $\mathbf{e}^A_{ij}$, which is uniform at large distances from the inclusion, as

$$\mathbf{e}^A_{ij} = \begin{pmatrix} -\nu & 0 & 0 \\ 0 & -\nu & 0 \\ 0 & 0 & 1 \end{pmatrix} \mathbf{e}^A \tag{18}$$

where $\mathbf{e}^A$ is given by σ^A/E. We want to obtain how this elastic field is perturbed by an oblate inclusion which has different elastic constants from those of matrix.

5-1. Internal Stress within the Inclusion, $(\sigma^I_{ij})_{inh}$

Eshelby [8] solved the inhomogeneity effect for an ellipsoidal inclusion in the matrix under an applied stress. He showed that internal stress within the inclusion, $(\sigma^I_{ij})_{inh}$, can be written as Eq. (19) instead of Eq. (2).

$$(\sigma^I_{ij})_{inh} = C_{ijk\ell}(\mathbf{e}^C_{k\ell} + \mathbf{e}^A_{k\ell} - \mathbf{e}^T_{k\ell}) = C^*_{ijk\ell}(\mathbf{e}^C_{k\ell} + \mathbf{e}^A_{k\ell}). \tag{19}$$

From Eqs. (18) and (19), $\mathbf{e}^T_{ij}$ for the inhomogeneity effect are obtained taking

$\nu = \nu^* = 1/3$ as,

$$\left.\begin{aligned} e^T_{11} = e^T_{22} = x_{mis} &= \frac{(1-m)\{(1-m)\,r(k) - 1\}}{3\{(1-m)^2 f(k) - (1-m)\,g(k) + 1\}} \cdot e^A \\ e^T_{33} = z_{inh} &= \frac{(1-m)\{3 - (1-m)\,s(k)\}}{3\{(1-m)^2 f(k) - (1-m)\,g(k) + 1\}} \cdot e^A \end{aligned}\right\} \quad (20)$$

and

$$e^T_{ij} = 0 \quad \text{if } i \neq j$$

where $r(k) = 3S_{1133} + S_{3333}$ and $s(k) = 3S_{1111} + 3S_{1122} + 2S_{3311}$. Numerical values of r and s are presented in Fig. 7.

The resultant $(\sigma^I_{ij})_{inh}$ can be written as

$$\left.\begin{aligned} (\sigma^I_{11})_{inh} = (\sigma^I_{22})_{inh} &= 2\mu^* \cdot \frac{1}{(1-m)} \cdot (3x_{inh} + z_{inh}) \\ (\sigma^I_{33})_{inh} &= 4\mu^* \cdot \frac{1}{(1-m)} \cdot (x_{inh} + z_{inh}) \end{aligned}\right\} \quad (21)$$

and

$$(\sigma^I_{ij})_{inh} = 0 \quad \text{if } i \neq j\ .$$

By using x_{inh} and z_{inh} in Eq. (20), the internal stresses were calculated as a function of k. The results are plotted against k in Figs. 8 and 9 for five different values of m. The stresses were normalized by σ^A. When m = 1, one obtains $(\sigma^I_{11})_{inh} = 0$ and $(\sigma^I_{33})_{inh} = \sigma^A$, which coincide with the applied stress. $(\sigma^I_{33})_{inh}$ becomes equal to σ^A when k vanishes regardless of m. As k approaches unity, the effect of m on $(\sigma^I_{33})_{inh}$ increases. By ploting $(\sigma^I_{33})_{inh}$ for $k > 1$, it can be shown that the stress approaches an asymptotic value depending on m at $k = \infty$. On the other hand, $(\sigma^I_{11})_{inh}$ approaches an asymptotic value as k goes to zero (see Fig. 8). Note that the ratio $(\sigma^I_{11})_{inh}/\sigma^A$ becomes

negative when the inclusion is stiffer than the matrix ($m > 1$). This ratio remains positive for $m < 1$.

5-2. Stress Concentration at Matrix-Inclusion Boundary

When we consider the internal stress of the matrix due to the inhomogeneity effect, the most interesting stress compoent at the boundary is $(\sigma^M_{33})_{inh}$ at equator point A. This becomes equivalent to the stress intensity factor problem of Mode I crack opening, by putting $m = 0$. At equator point A, $\cos\theta$ in Eq. (5) is equal to 1, so σ^M_{33} in Eq. (6) becomes as

$$\sigma^M_{33} = \mu\{4(\mathbf{e}^c_{11} + \mathbf{e}^c_{33}) - 3x - z\} .$$

Hence, $(\sigma^M_{33})_{inh}$ at A can be written as,

$$(\sigma^M_{33})_{inh} = \frac{3}{8}\cdot E[\{4(S_{1111} + S_{1122} + 2S_{3311}) - 3\}x_{inh} + \{4(S_{3333} + S_{1133}) - 1\}z_{inh} + \frac{8}{3}\cdot\mathbf{e}^A] . \quad (22)$$

By substituting x_{inh} and z_{inh} from Eq. (19), $(\sigma^M_{33})_{inh}$ was calculated as a function of k. The results are prented in Fig. 10 for four different values of m. At $m = 0$, Eq. (22) becomes simply,

$$(\sigma^M_{33})_{inh}/\sigma^A = \frac{r(k) - 3s(k) + 8}{8\{1 + f(k) - g(k)\}} . \quad (23)$$

When k is zero, we have $f(0) = 0$, and $g(0) = r(0) = s(0) = 1$, so $(\sigma^M_{33})_{inh}/\sigma^A$ becomes infinte. At $k = 1$, we have $(\sigma^M_{33})_{inh}/\sigma^A = 2.0625$ with $\nu = 1/3$. When k becomes smaller than 0.01 at $m = 0$, $(\sigma^M_{33})_{inh}/\sigma^A$ can be approximated by $1.28/k$.

The radius of carvature for an ellipse in Fig. 1 is given by

$$\rho = \frac{\{a^4 + (c^2 - a^2)X_1^2\}^{3/2}}{a^4 c} \quad .$$

At equator point $A(X_1 = a)$, $\rho = c^2/a$, therefore $(\sigma_{33}^M)_{inh}$ for a flat cavity can be rewritten in terms of ρ as $(\sigma_{33}^M)_{inh} = 1.28 \times \sigma^A \times \sqrt{a/\rho}$. The stress intensity factor of "Mode I" crack opening is given as [3],

$$K_I = \lim_{\rho \to 0} \frac{\sqrt{\pi}}{2} \cdot (\sigma_{33}^M)_{inh} \sqrt{\rho} \quad .$$

By substituting $(\sigma_{33}^M)_{inh}$, K_I for a flat cavity can be written as,

$$K_I = \frac{1.28\sqrt{\pi}}{2} \cdot \sigma^A \sqrt{a} \approx 1.13 \sigma^A \sqrt{a} \quad .$$

This agrees with Sneddon's result for a penny-shaped crack [3,27]. The stress distribution around a spheroidal cavity was obtained by Neuber [5] for various types of stressing. In the case of simple tension in the direction of the axis of revolution $(\sigma_{33}^M)_{inh}/\sigma^A$ vs. a/ρ were plotted using three specific values of ν. Our corresponding result at $m = 0$ (Fig. 8) agrees well with his results taking $\nu = 0.3$.

The evaluation of $(\sigma_{33}^M)_{inh}$ for an inclusion ($m \neq 0$) is important in relation to fatigue and brittle fracture. As can be seen in Fig. 10, $(\sigma_{33}^M)_{inh}$ decreases with increases in the value of m. Its dependence on m at a given k becomes quite large as k decreases. When k is equal to zero, $(\sigma_{33}^M)_{inh}$ can be written as,

$$(\sigma_{33}^M)_{inh} = \frac{(3 - m)(1 + m)}{4m} \cdot \sigma^A \quad . \qquad (24)$$

Using Eq. (24), values of m at selected ratios of $(\sigma^M_{33})_{inh}/\sigma^A$ were obtained and listed below:

m	0	0.07	0.46	1	3	10.3	38	∞
$(\sigma^M_{33})_{inh}/\sigma^A$	∞	10	2	1	0	-2	-10	$-\infty$

It can be seen that the stress concentration factor becomes less than 2 when the shear modulus ratio m is between 0.46 and 10.3. Note that when m is greater than 3, the sign of the stress ratio becomes negative; i.e., when a compressional stress is applied, a large tensile stress results at equator point A for a thin disc inclusion having a large m value.

Edwards [6] evaluated the stress concentration factor of prolate spheroidal inclusion ($k \geq 1$). Our results in Fig. 10 agree well with his at $k = 1$.

6. PLASTIC DEFORMATION EFFECT

Suppose a plastically non-deformable inclusion exists in a deformable matrix. When applied stress deforms the matrix plastically internal stresses develop around the inclusion. Tanaka and Mori [9] evaluated such internal stresses and developed a work-hardening theory of composite materials by using Eshelby's method. However, only the limiting cases were considered. In order to compliment the present calculations, it is necessary to evaluate effects of k for quantitative analysis of the plastic deformation effect. Following Tanaka and Mori [9], the uniform plastic deformation of the matrix proceeds by multiple glide, producing uniaxial strain ε_p along x_3 axis. The geometry of an inclusion is that given in Fig. 1. We can write a stress-free transformation strain inside the inclusion as follows:

$$e_{ij}^{T*} = \begin{pmatrix} 1/2 & 0 & 0 \\ 0 & 1/2 & 0 \\ 0 & 0 & -1 \end{pmatrix} \varepsilon_p \, . \qquad (25)$$

Ashby [28] first described the equivalent condition by using a dislocation concept; i.e., the generation of dislocation loops at the interface of the inclusion. In the method of Tanaka and Mori, the elastic fields are obtained by employing Eq. (2). Note that as a consequence of the stress free strain [Eq. (25)], a spheroidal inclusion with the aspect ratio k is to be considered as the one with $k' = k(1 + \frac{3}{2} \cdot \varepsilon_p)$ for the first approximation [9].

6-1. Internal Stress Within the Inclusion, $(\sigma_{ij}^I)_p$

e_{ij}^T in Eq. (2) for plastic deformation effect can be expressed as

$$\left.\begin{aligned} e_{11}^T = e_{22}^T = x_p &= \frac{m\{1 - (1 - m)u(k)\}}{2\{(1 - m)^2 f(k) - (1 - m)\, g(k) + 1\}} \cdot \varepsilon_p \\ e_{33}^T = z_p &= \frac{m\{(1 - m)\, v(k) - 1\}}{\{(1 - m)^2\, f(k) - (1 - m)\, g(k) + 1\}} \cdot \varepsilon_p \end{aligned}\right\} \qquad (26)$$

where $u(k) = 2S_{1133} + S_{3333}$ and $v(k) = S_{1111} + S_{1122} + S_{3311}$ (see Fig. 7). Internal stress within the inclusion, $(\sigma_{ij}^I)_p$, can be calculated. The results indicate that $(\sigma_{ij}^I)_p = 0$ if $i \neq j$, and the diagonal stress components are,

$$\left.\begin{aligned} (\sigma_{11}^I)_p = (\sigma_{22}^I)_p &= 2\mu^* \cdot \frac{1}{(1 - m)} \cdot \{(3x_p + z_p) - \varepsilon_p/2\} \\ (\sigma_{33}^I)_p &= 4\mu^* \cdot \frac{1}{(1 - m)} \cdot \{(x_p + z_p) + \varepsilon_p/2\} \, . \end{aligned}\right\} \qquad (27)$$

Numerical results are presented in Fig. 11[†] and Fig. 12[†], where the stresses are normalized by the factor $E^* \cdot \varepsilon_p$. As k goes to 0 (disc), each of $(\sigma^I_{11})_p/E^* \cdot \varepsilon_p$ and $(\sigma^I_{33})_p/E^* \cdot \varepsilon_p$ approaches to an asymptotic value; -0.75 and 0, respectively. As k goes to 1 (sphere) at constant m, the magnitude of $(\sigma^I_{11})_p$ decreases, but that of $(\sigma^I_{33})_p$ increases. At k = 1, we have $(\sigma^I_{33})_p = 2(\sigma^I_{11})_p$ for a given m [10].

6-2 Internal Stress at the Boundary, $(\sigma^M_{ij})_p$

As the amount of plastic deformation of the matrix is increased, the internal stress at the matrix-inclusion boundary develops according to Eq. (6). For example, an internal stress component, $(\sigma^M_{33})_p$, at equator point A can be written as

$$(\sigma^M_{33})_p = \frac{3}{8} E[\{4(S_{1111} + S_{1122} + 2S_{3311}) - 3\}x_p + \{4(S_{3333} + S_{1133}) - 1\}z_p] \quad .$$

The identical component at polar point B is given by

$$(\sigma^M_{33})_p = \frac{3}{2} \cdot E \cdot \frac{m}{(1 - m)} \cdot \{(x_p + z_p) + \varepsilon_p/2\} \quad .$$

Figure 13 shows the results obtained by substituting x_p and z_p from Eq. (26). At polar point B, we have $\sigma^I_{33} = \sigma^M_{33}$. At equator point A, $(\sigma^M_{33})_p/E \cdot \varepsilon_p$ depends on the values of m and k. When $m \geq 1$, the maximum of $(\sigma^m_{33})_p$ occurs at k = 0. In this case, the thinner is the inclusion, the smaller amount of ε_p will initiate the decohesion at the boundary. On the other hand, when

[†]The horizontal axis in the figures is to be $k' = k(1 + 3\varepsilon_p/2)$, however, if ε_p is less than 6%, the difference between k' and k becomes less than 10%.

$m < 1$, the maximum stress is reached with $0 < k < 1$; for example, the maximum of $(\sigma^M_{33})_p$ occurs at $k \simeq 0.2$ when $m = 0.5$.

As in the cases discussed in Sections 4 and 5, not all the non-diagonal components of $(\sigma^M_{ij})_p$ vanish. Thus, shear stresses at the boundary can be deduced, although extended computations are required. In the case of a spherical inclusion, Mori and coworkers [29] determined the shear stresses and their maxima at the boundary. They employed the calculation in the analysis of plastic relaxation around a particle.

7. DISCUSSION

The present study has evaluated the internal stresses within inclusion, σ^I_{ij}, and those at the matrix-inclusion boundary, σ^M_{ij}, due to the misfit, inhomogeneity, and plastic deformation effects. Specifically, $\sigma^I_{11} = \sigma^I_{22}$, σ^I_{33} and σ^M_{33} have been obtained as a function of k and m for an oblate spheroidal inclusion. Now, one can obtain the internal stresses once the values of m and k are known. While the orientation of the inclusion has no essential effect on the misfit induced stresses because of isotropy, the inhomogeneity and plastic deformation effects are limited to the specific geometry considered. In the present study, the direction of external stress σ^A coincides the axis of revolution of the inclusion, which is also the direction of uniaxial plastic strain ε_p.

Within the limits of the present calculation, a variety of problems in materials research can be analyzed in addition to those examined in the previous sections of this paper. Since mechanical responses of inclusions in structural materials are of significant concern, we consider as an example the internal stresses in and around an MnS inclusion in steel.

It is well known that the decohesion of flattened oblong-shaped MnS inlcusions in steel plates is responsible for the loss of ductility along the thickness direction. The loss is particularly pronounced when the recently developed controlled rolling process is adopted. Acoustic emission studies of high strength low alloy steels have revealed that the decohesion or fracture of the inclusions takes place well before the yield stress is reached. [30,31]. Much of decohesion are complete within the initial several percent of plastic deformation. Let us consider the stress in and around an MnS inclusion. Its shape is approximated by an oblate spheroid and the applied stress is along the axis of revolution. It is assumed that the matrix ceases to allow plastic relaxation around the inclusion below 800°K, giving rise to thermal misfit strain. The thermal expansion coefficients of MnS and steel are found to be 18.1 x 10^{-6}/°K and 12.0 x 10^{-6}/°K, respectively [32], which gives $\varepsilon^T = -3 \times 10^{-3}$. Young's moduli of MnS and steel are 137 GPa and 206 GPa, respectively, which correspond to m = 2/3 [32]. The magnitude of σ^A was taken as E/1000 or 206 MPa. The amount of ε_p was set at 0.1% or 1%, although σ^A would be higher than E/1000 when the latter value was employed.

The internal stress σ^I_{33} inside the MnS inclusion was calculated for the three different effects (cf. Eqs. 8, 21 and 27). The results are presented against k in Fig. 14. Individual components as well as the sum of the three, $(\sigma^I_{33})_{total} = (\sigma^I_{33})_{mis} + (\sigma^I_{33})_{inh} + (\sigma^I_{33})_p$, are given. As k approaches zero, the contributions of $(\sigma^I_{33})_{mis}$ and $(\sigma^I_{33})_p$ become negligible. Plastic deformation effect is small regardless of k until ε_p exceeds several percent. Misfit effect becomes significant as k increases; $(\sigma^I_{33})_{mis}$ exceeds $(\sigma^I_{33})_{inh}$ for $K > 0.18$. For a typical aspect ratio of MnS inclusions of about 0.1, both misfit and inhomogeneity effects produce the normal stress on the broad face of the inclusion. The internal stress σ^M_{33} at equator point A of the matrix-inclusion boundary was also obtained by using Eqs. (6) and (22). The results

are shown in Fig. 15. As can be seen in Fig. 15, the total internal stress at point A, $(\sigma^M_{33})_{total} = (\sigma^M_{33})_{mis} + (\sigma^M_{33})_{inh} + (\sigma^M_{33})_p$, is negative as far as ε_p is less than 2%. This is due to a large negative values of the misfit effect. If $(\sigma^M_{33})_{mis}$ remains unrelaxed by plastic deformation of the matrix, it is most unlikely that the decohesion or fracture begins at the edge of an inclusion. Even if some plastic relaxation occurs, the present analysis indicates that the normal stress on the inclusion plane, $(\sigma^I_{33})_{inh}$ and $(\sigma^I_{33})_{mis}$ in particular, contributes most significantly to the decohesion of the inclusion.

Tanaka et al. [10,11] were the first to apply Eshelby theory to the decohesion problem. However, misfit effect was not included. When a spherical inclusion is considered, their conclusion is basically valid. Because of the omission of the misfit effect, the contribution of plastic deformation effect appears to be overemphasized. In dealing with the disc-shaped inclusions, however, the geometry was inappropriate in that the decohesion was considered to occur at the edge of the an infinitely thin inclusion via σ^I_{11}. Again, the plastic deformation effect was overestimated. Thus, their conclusion concerning disc-shaped inclusions is inapplicable to configurations of general interest.

REFERENCES

(1) N. F. Mott and F.R.N. Nabarro, Proc. Phys. Soc. London 52, 86 (1940).

(2) R. E. Peterson, Stress Concentration Design Factors, p. 137, John Wiley, New York (1953).

(3) P. Paris and G. Sih, Fracture Toughness Testing and Its Application, ASTM-STP 381, p. 30 (1964).

(4) M. A. Sadowsky and E. Sternberg, J. Appl. Mech., Trans. ASME 69, A-191 (1947).

(5) H. Neuber, Kerbspannugslehre, p. 120, Springer, Berlin (1937).

(6) R. H. Edwards, J. Appl. Mech., Trans. ASME 55, 39 (1933).

(7) L. Mirandy and B. Paul, J. Engr. Materials and Tech., Trans. ASME 2, 164, (1976).

(8) J. D. Eshelby, Proc. Roy. Soc. A241, 376 (1957).

(9) K. Tanaka and T. Mori, Acta Met. 18, 931 (1970).

(10) K. Tanaka, T. Mori, and T. Nakamura, Phil. Mag. 21, 267 (1970).

(11) K. Tanaka, T. Mori, and T. Nakamura, Trans. Iron and Steel Inst. Japan 11, 383 (1971).

(12) K. Tanaka and S. Matsuoka, Acta Met. 22, 153 (1974).

(13) L. M. Brown and D. R. Clarke, Acta Mat. 23, 821 (1975).

(14) J. K. Lee, D. M. Barnett and H. I. Aaronson, Met. Trans. 8A, 963 (1977).

(15) K. Robinson, J. Appl. Phys. 3, 79 (1956).

(16) D. M. Barnett, J. K. Lee, H. I. Aaronson, and K. C. Russell, Scripta Met. 8, 1447 (1974).

(17) A. E. Love, A Treatise on the Mathematical Theory of Elasticity, p. 187, Dover, New York (1944).

(18) J. D. Eshelby, Phil. Trans. A244, 87 (1951).

(19) C. Zener, Phys. Rev. 74, 639 (1948).

(20) H. Kayano, Trans. Japan Inst. Metal 9, 156 (1968).

(21) J. W. Mitchell, Growth and Perfection of Crystals, p. 386, John Wiley, New York (1958).

(22) A. Lawley and H. L. Gaigher, Phil. Mag. 8, 1713 (1963).

(23) A. H. Cottrell, Dislocations and Plastic Flow in Crystals, p. 11, Clarendon Press, Oxford (1953).

(24) H. B. Huntington, Solid State Phys. 7, 213 (1958)

(25) P. Shaffer, Plenum Press Handbook of High Temperature Materials, pp. 99-381, Plenum Press, New York (1964).

(26) E. B. Shand, Glass Engineering Handbook, P. 18, McGraw-Hill, New York (1958).

(27) L. N. Sneddon, Proc. Roy. Soc. London A187, 229 (1946).

(28) M. F. Ashby, Proc. Second Bolton Landing Conf. on Oxide Dispersion Strengthening, p. 143, Gordon and Breach, New York (1968).

(29) K. Tanaka, K. Narita and T. Mori, Acta Met. 20, 297 (1972).

(30) K. Ono, G. Huang and H. Hatano, Proc. 8th World Conf. NDT, Cannes, France, Paper No. 3K3, September 1976 .

(31) K. Ono, G. Huang and A. Kawamoto, Proc. 6th Int. Conf. on Internal Friction and Ultrasonic Attenuation in Solid, Tokyo, Japan, July 1977 .

(32) J. Tsuboi and M. Hirai, Kawasaki Steel Corp. Tech. Rep., October 1974 .

Reference	Matrix	Inclusion	$\mu/10$ (GPa)	$\mu^*/10$ (GPa)	$10^6\ \alpha$ ($^\circ K^{-1}$)	$10^6\ \alpha^*$ ($^\circ K^{-1}$)	$-\Delta T$ ($^\circ K$)	$10^2\ \varepsilon^T$	τ^M_{max}/μ [Eq. (13)]	Dislocation around inclusion
[20]	Fe	Al_2O_3	7.3[24]	15.6[25]	15.1[25]	8.0[25]	780	0.55	$\frac{1}{75}$	None
		ZrO_2	7.3[24]	6.9[25]	15.1[25]	7.2[25]	780	0.62	$\frac{1}{82}$	Irregular Arrangement
[21]	AgCl	Borosilicate Glass	1.2[24]	2.5[26]	34.5[21]	3.4[21]	400	1.24	$\frac{1}{33}$	Prismatic -Loops
[22]	Mo	Mo_2C	14.2[24]	8.7[25]	7.5[25]	6.2[25]	2380	0.31	$\frac{1}{196}$	Prismatic -Loops

TABLE I

Maximum Shear Stress of the Matrix around
a Spherical Inclusion

FIGURE CAPTIONS

Fig. 1. The orientation of an oblate spheroidal inclusion. Applied stress, σ^A, is exerted along the X_3. Equator point A refers to $X_1^2 + X_1^2 = a^2$ and polar point B refers to (0,0,c).

Fig. 2. Shape dependence of parametric functions; f, g, h and ℓ.

Fig. 3. Normal components of internal stress (normalized by $E^*\varepsilon^T$) inside the inclusion due to misfit effect vs. aspect ratio, k. The ratio of Young's moduli employed is indicated.

Fig. 4. Maximum shear stress inside the inclusion due to misfit effect. $\tau^I_{mis}/\mu^*\varepsilon^T$ against k.

Fig. 5. Elastic strain energy of the inclusion and matrix due to misfit effect. $E_s/4\mu^*(\varepsilon^T)^2V_I$ against k.

Fig. 6. Internal stress at the matrix-inclusion boundary due to misfit effect. $(\sigma^M_{33})_{mis}/E\varepsilon^T$ against k.

Fig. 7. Shape dependence of parametric functions; r, s, u and v.

Fig. 8. Internal stress inside the inclusion due to inhomogeneity effect. $(\sigma^I_{11})_{inh}/\sigma^A$ against k.

Fig. 9. Internal stress inside the inclusion due to inhomogeneity effect. $(\sigma^I_{33})_{inh}/\sigma^A$ against k.

Fig. 10. Internal stress at the equator point A on the matrix-inclusion boundary due to inhomogeneity effect. $(\sigma^M_{33})_{inh}/\sigma^A$ against k.

Fig. 11. Internal stress inside the inclusion due to uniaxial plastic deformation of the matrix. $(\sigma^I_{11})_p/E^*\varepsilon_p$ against k.

Fig. 12. Internal stress inside the inclusion due to plastic deformation effect. $(\sigma^I_{33})_p/E^*\varepsilon_p$ against k.

Fig. 13. Internal stress at equator point A and polar point B at the matrix-inclusion boundary due to plastic deformation effect. $\sigma^M_{33}/E\varepsilon_p$ against k.

Fig. 14. Internal stress inside an oblate MnS inclusion in the steel matrix (m = 2/3). Three components of σ_{33}^{I} and their sum for the case of ε_p = 1% are shown against k. σ^{A} was taken as $10^{-3}E$ or $1.5 \times 10^{-3}E^{*}$.

Fig. 15. Internal stress at equator point A of the matrix-inclusion boundary. σ_{33}^{M}/E against k. Note a large negative contribution due to misfit effect.

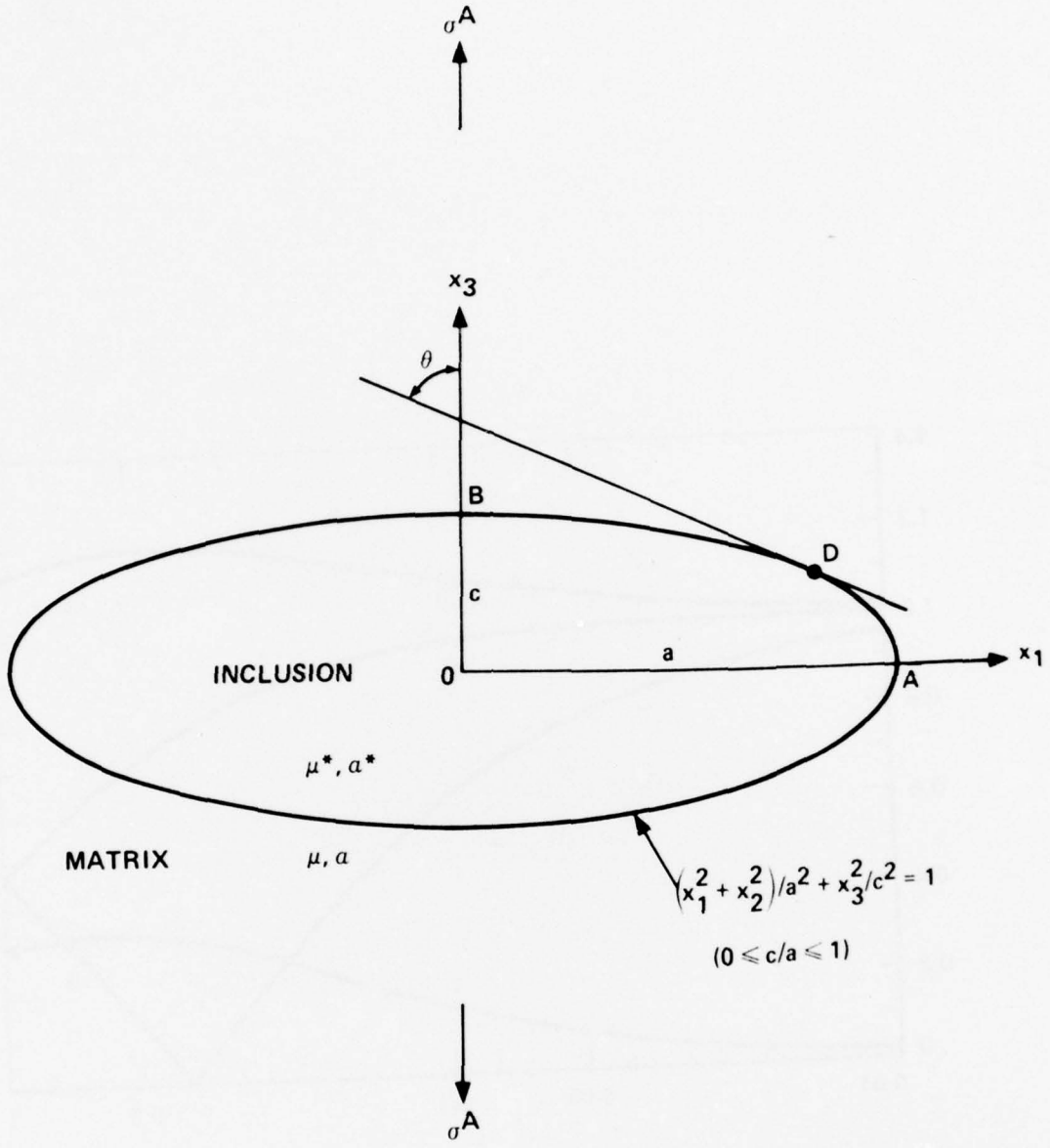

Fig. 1. The orientation of an oblate spheroidal inclusion. Applied stress, σ^A, is exerted along the X_3. Equator point A refers to $X_1^2 + X_2^2 = a^2$ and polar point B refers to (0,0,c).

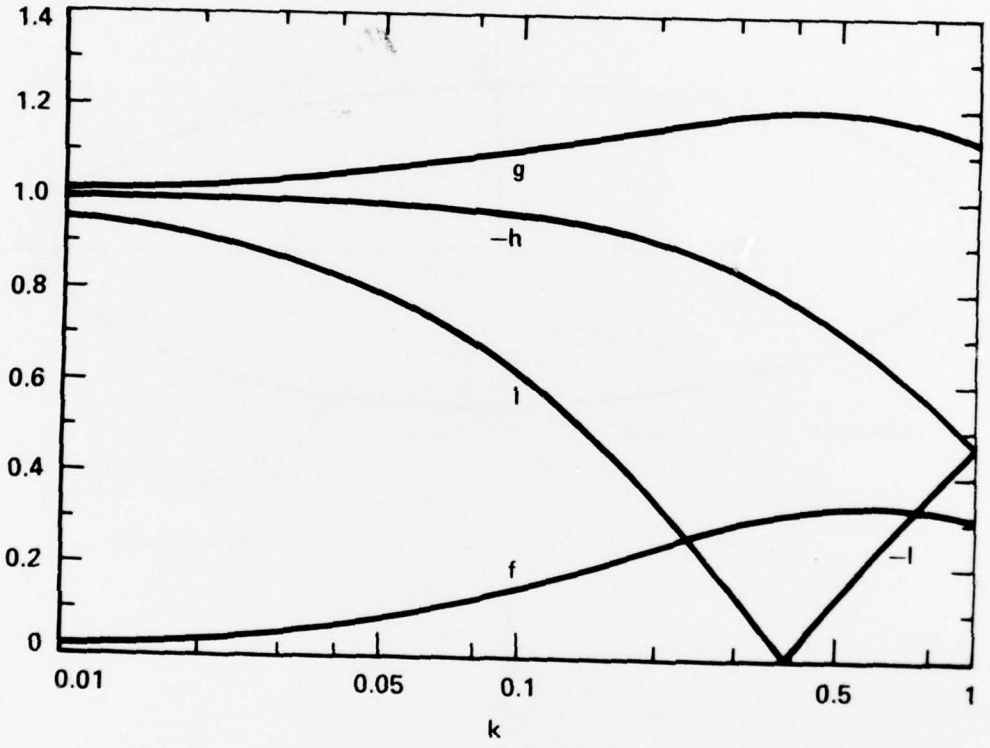

Fig. 2. Shape dependence of parametric functions; f, g, h and ℓ.

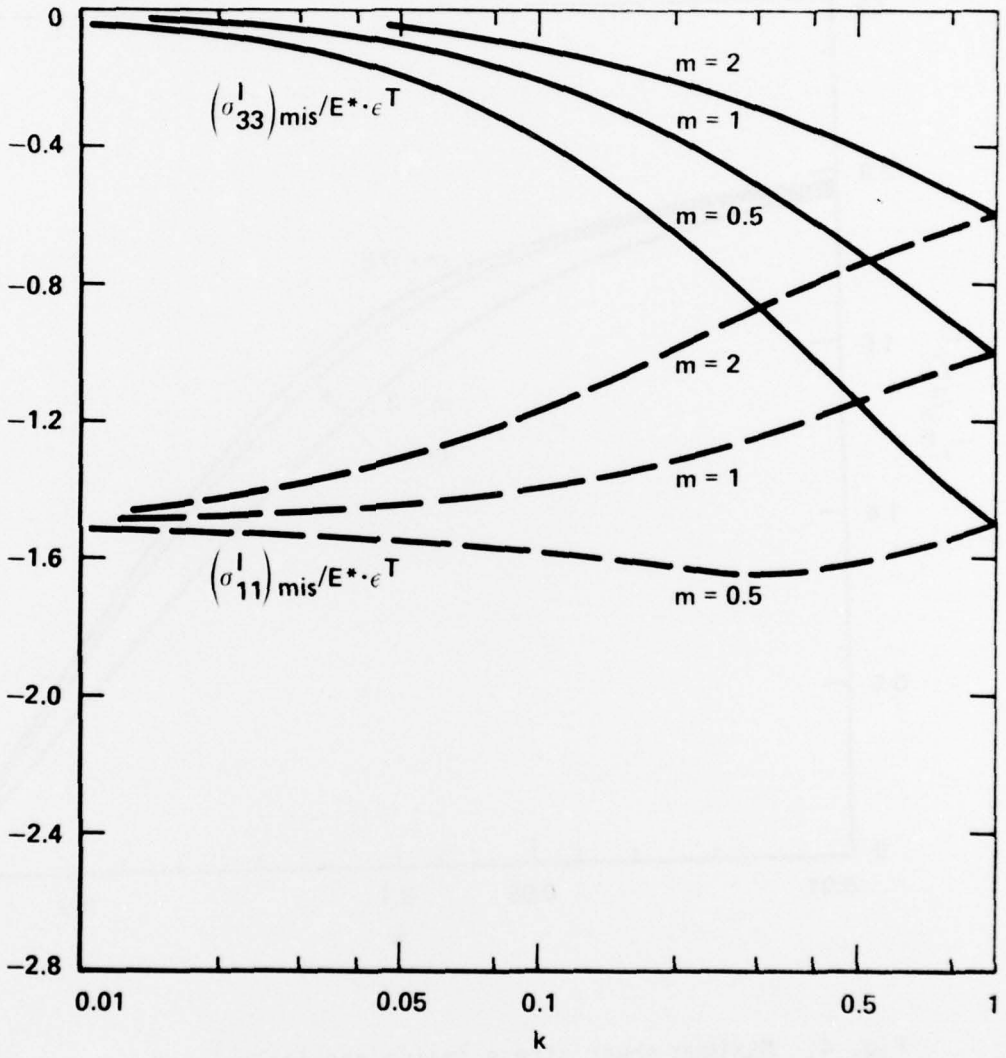

Fig. 3. Normal components of internal stress (normalized by $E^{*}\epsilon^{T}$) inside the inclusion due to misfit effect vs. aspect ratio, k. The ratio of Young's moduli employed is indicated.

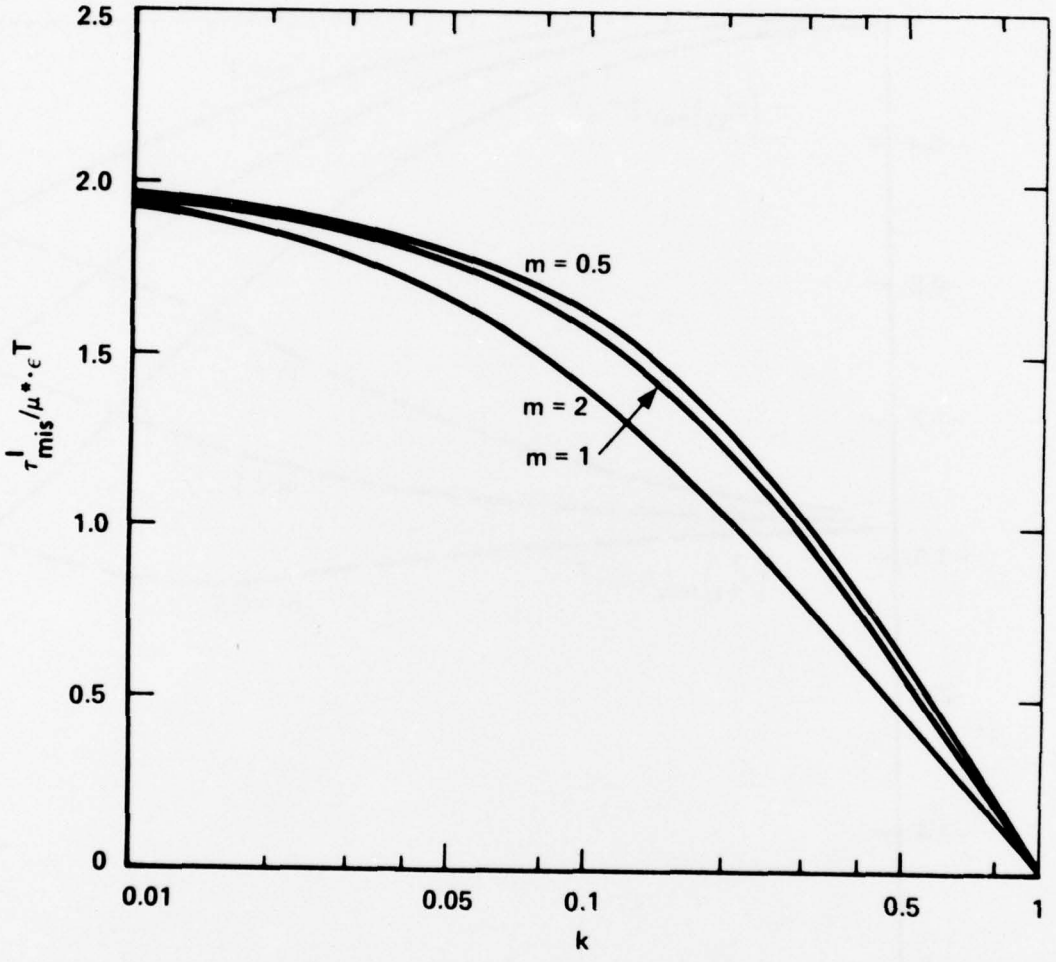

Fig. 4. Maximum shear stress inside the inclusion due to misfit effect. $\tau^I_{mis}/\mu^*\varepsilon^T$ against k.

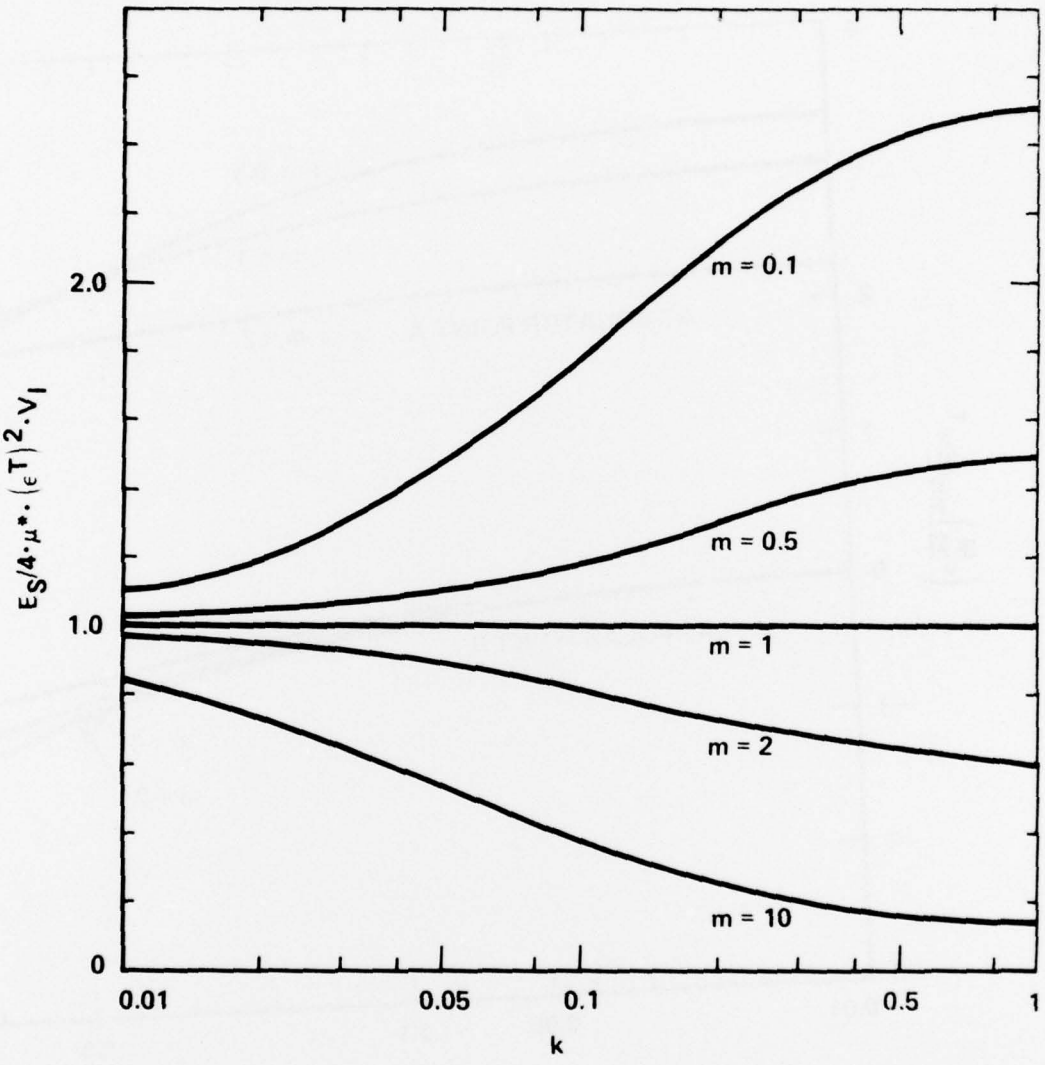

Fig. 5. Elastic strain energy of the inclusion and matrix due to misfit effect. $E_s/4\mu^*(\varepsilon^T)^2V_I$ against k.

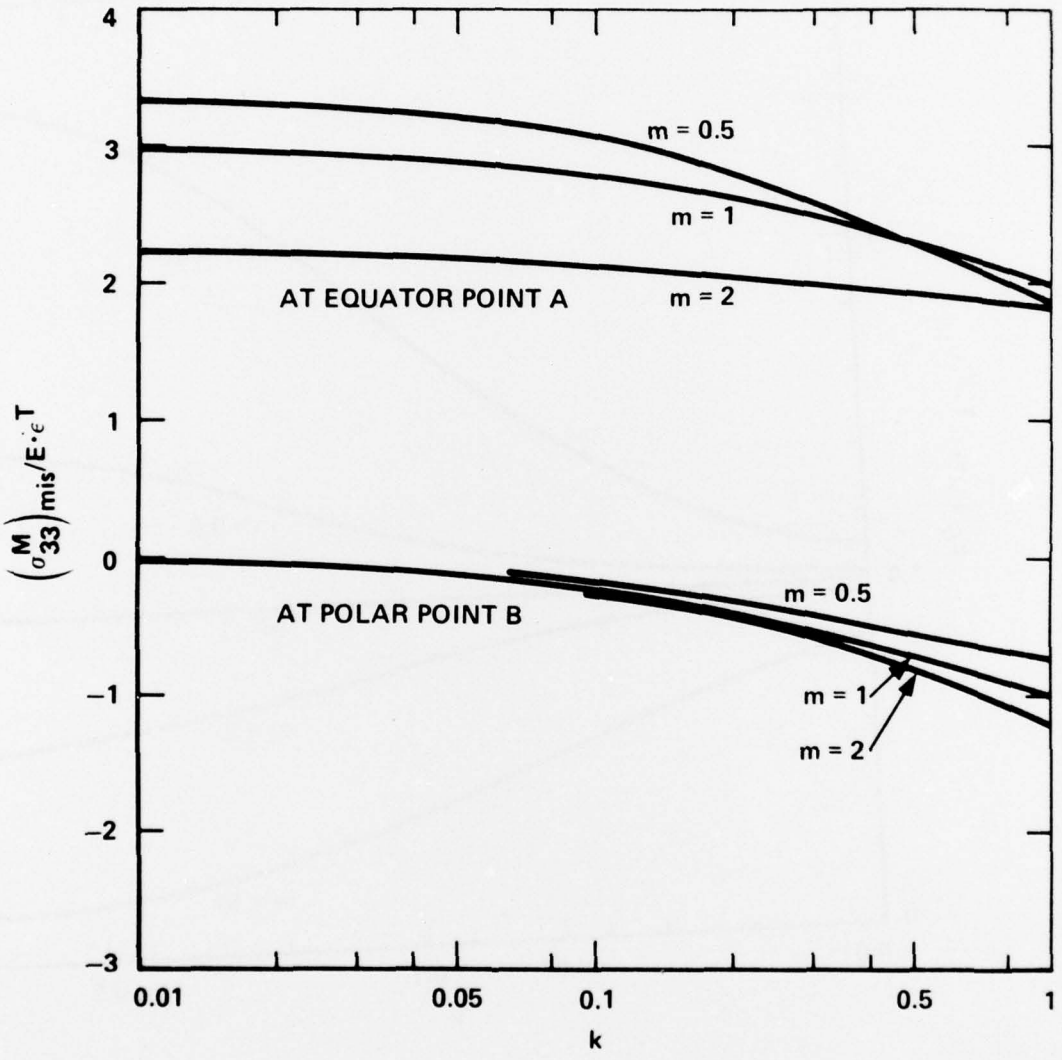

Fig. 6. Internal stress at the matrix-inclusion boundary due to misfit effect. $(\sigma_{33}^{M})_{mis}/E\epsilon^{T}$ against k.

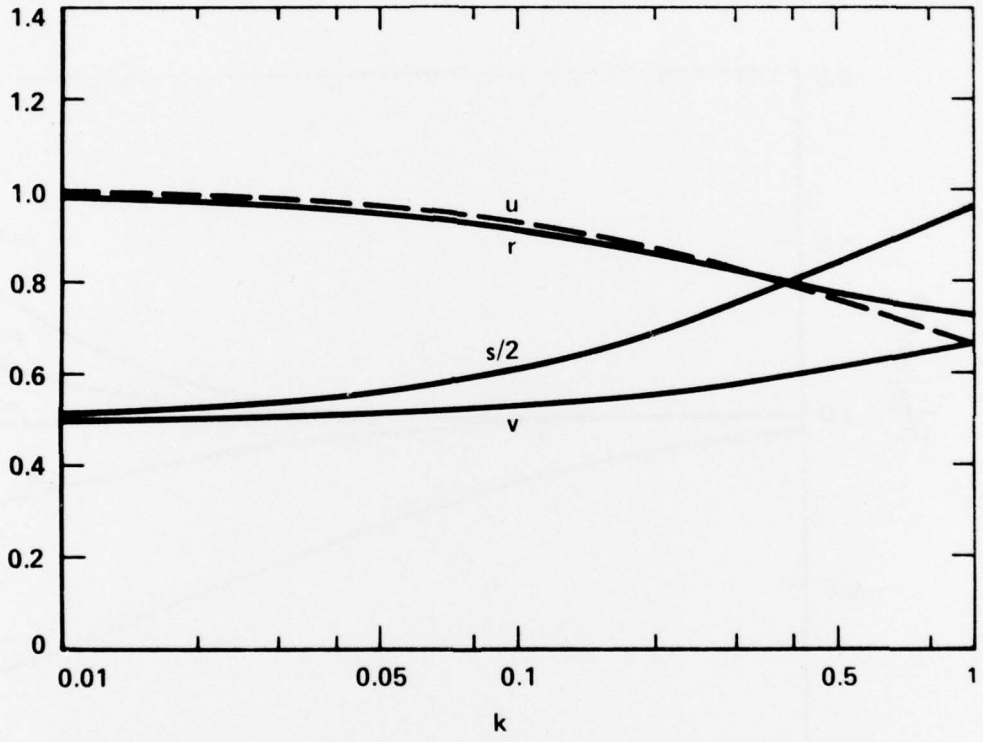

Fig. 7. Shape dependence of parametric functions; r, s , u and v.

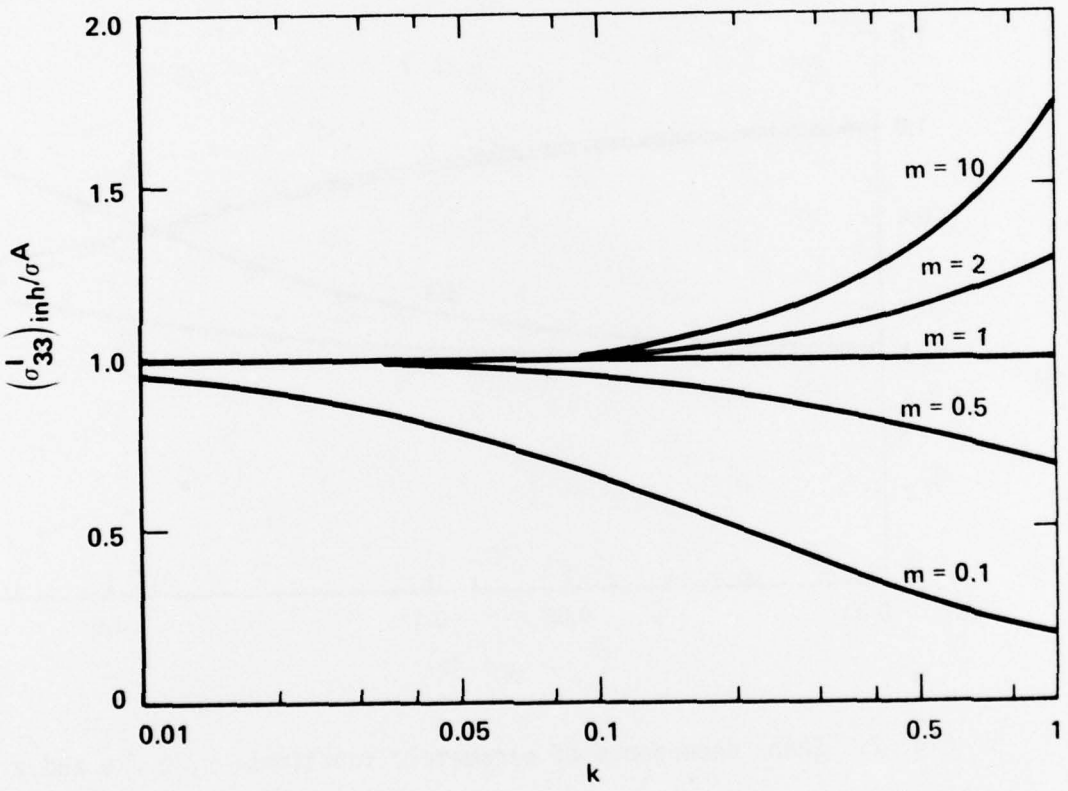

Fig. 8. Internal stress inside the inclusion due to inhomogeneity effect. $(\sigma^I_{33})_{inh}/\sigma^A$ against k.

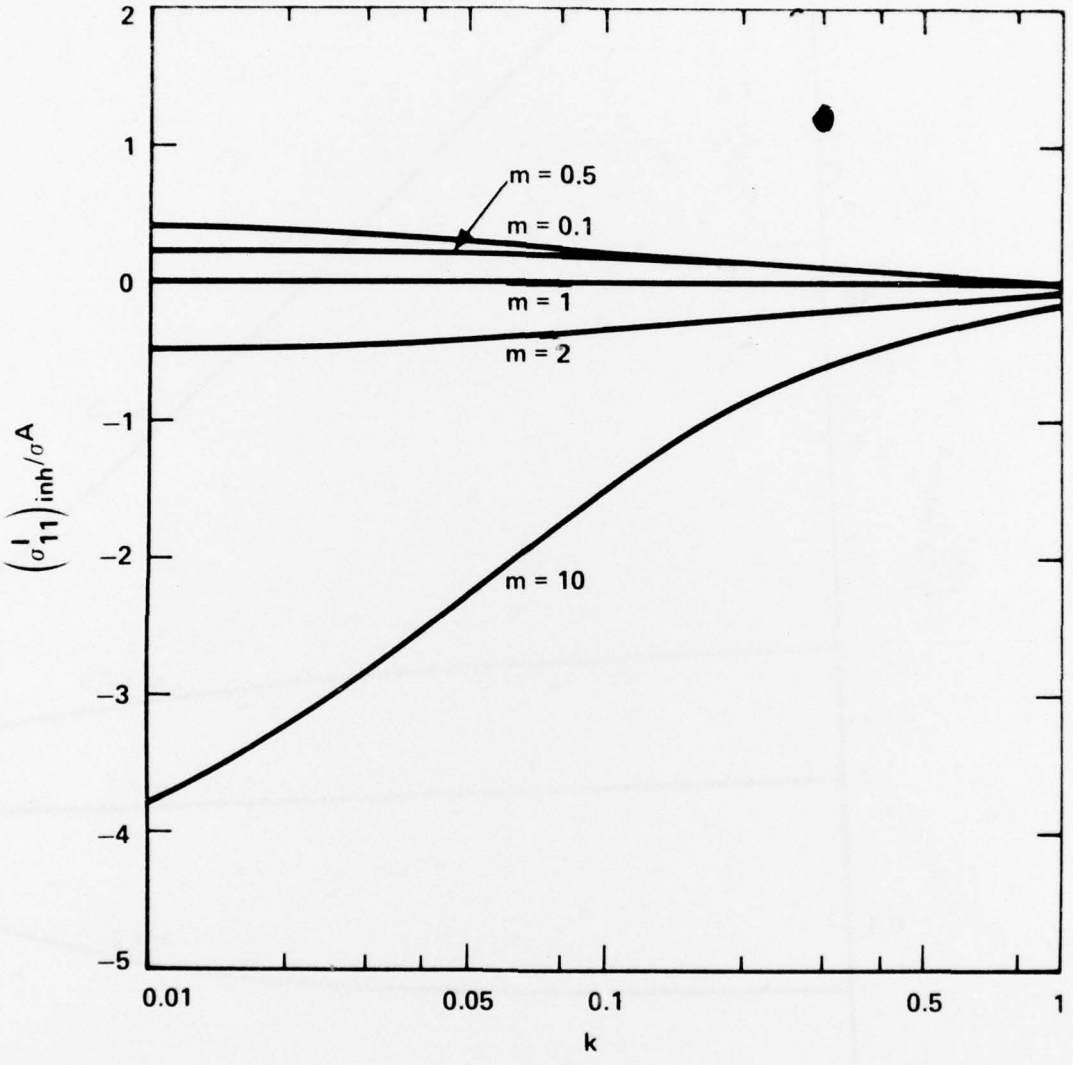

Fig. 9. Internal stress inside the inclusion due to inhomogeneity effect. $(\sigma^I_{11})_{inh}/\sigma^A$ against k.

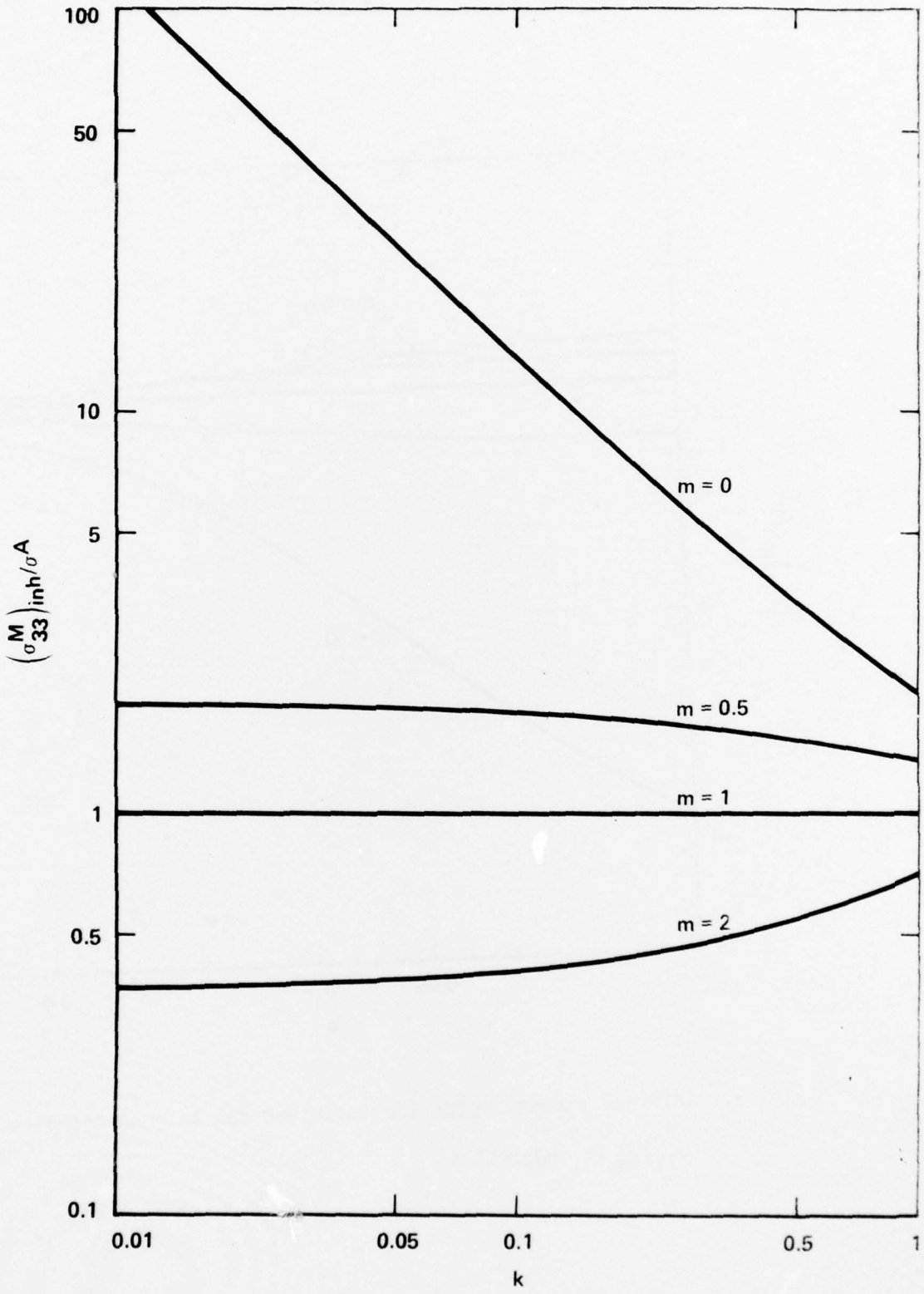

Fig. 10. Internal stress at the equator point A on the matrix-inclusion boundary due to inhomogeneity effect. $(\sigma_{33}^{M})_{inh}/\sigma^{A}$ against k.

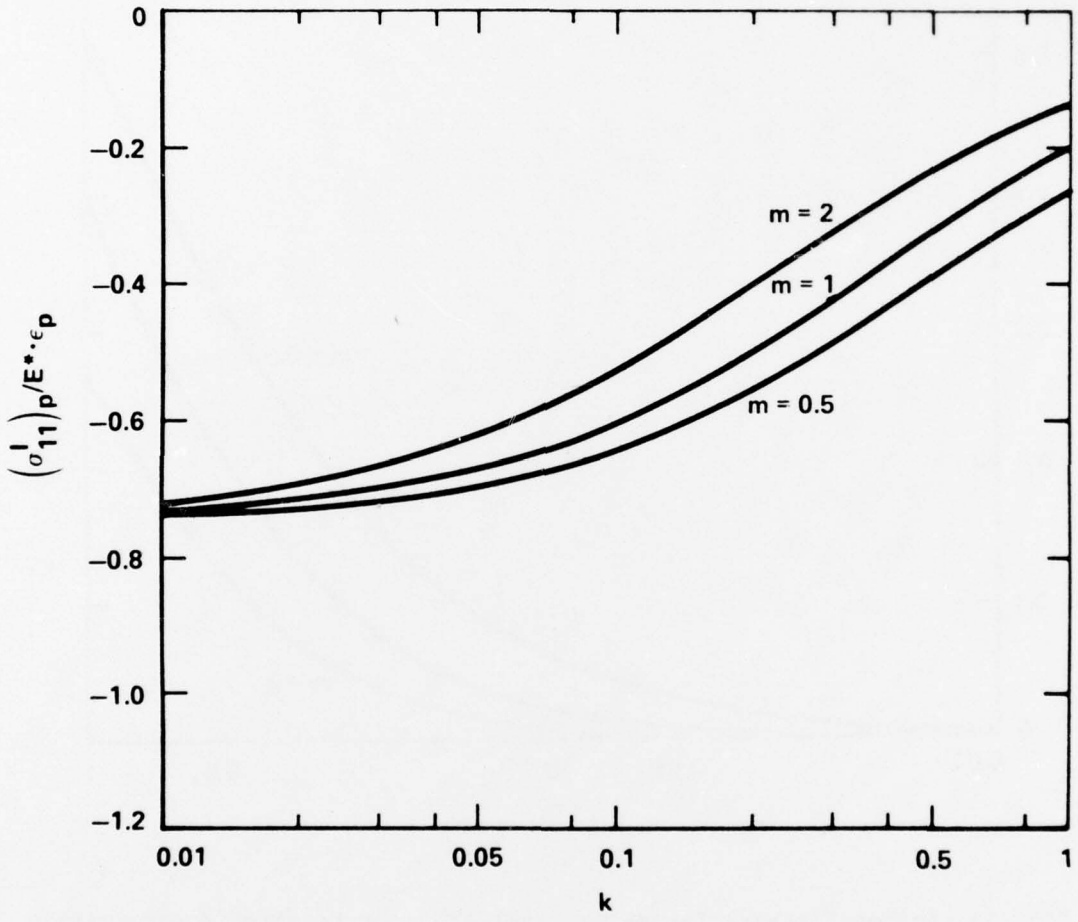

Fig. 11. Internal stress inside the inclusion due to uniaxial plastic deformation of the matrix. $(\sigma^I_{11})_p/E^*\varepsilon_p$ against k.

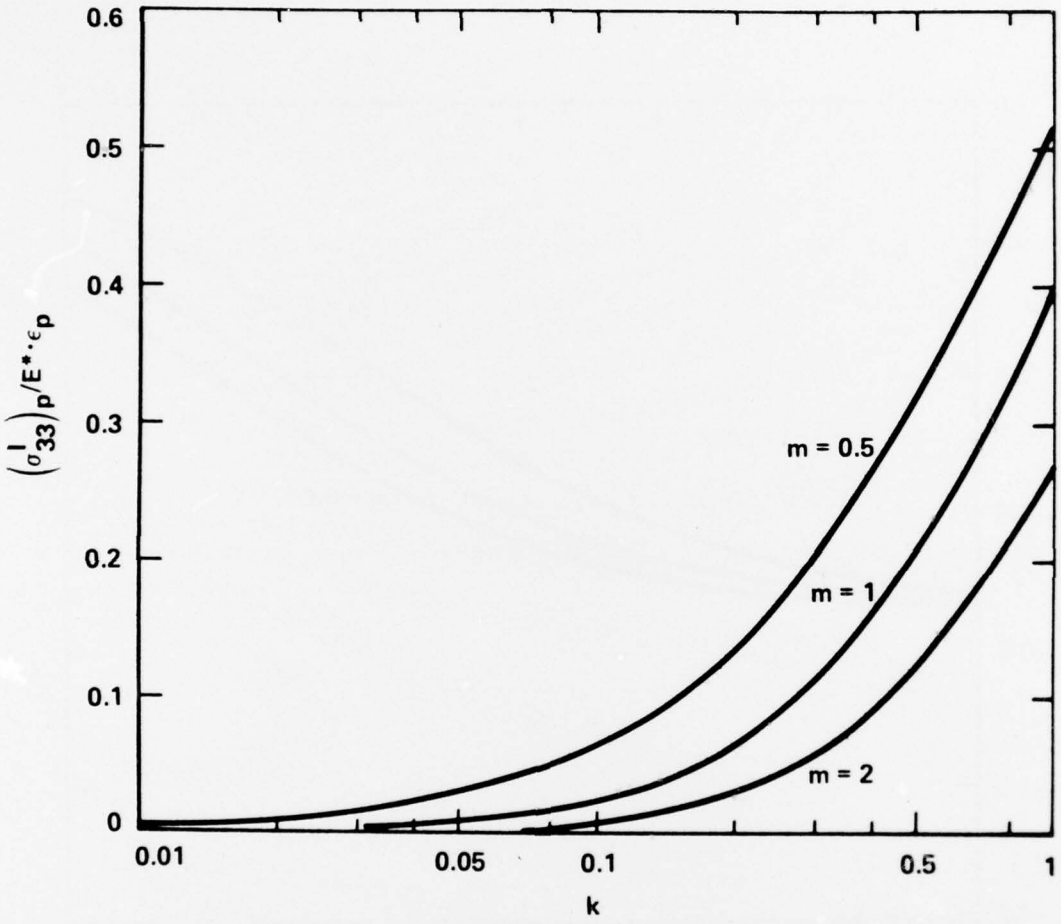

Fig. 12. Internal stress inside the inclusion due to plastic deformation effect. $(\sigma^I_{33})_p/E^* \epsilon_p$ against k.

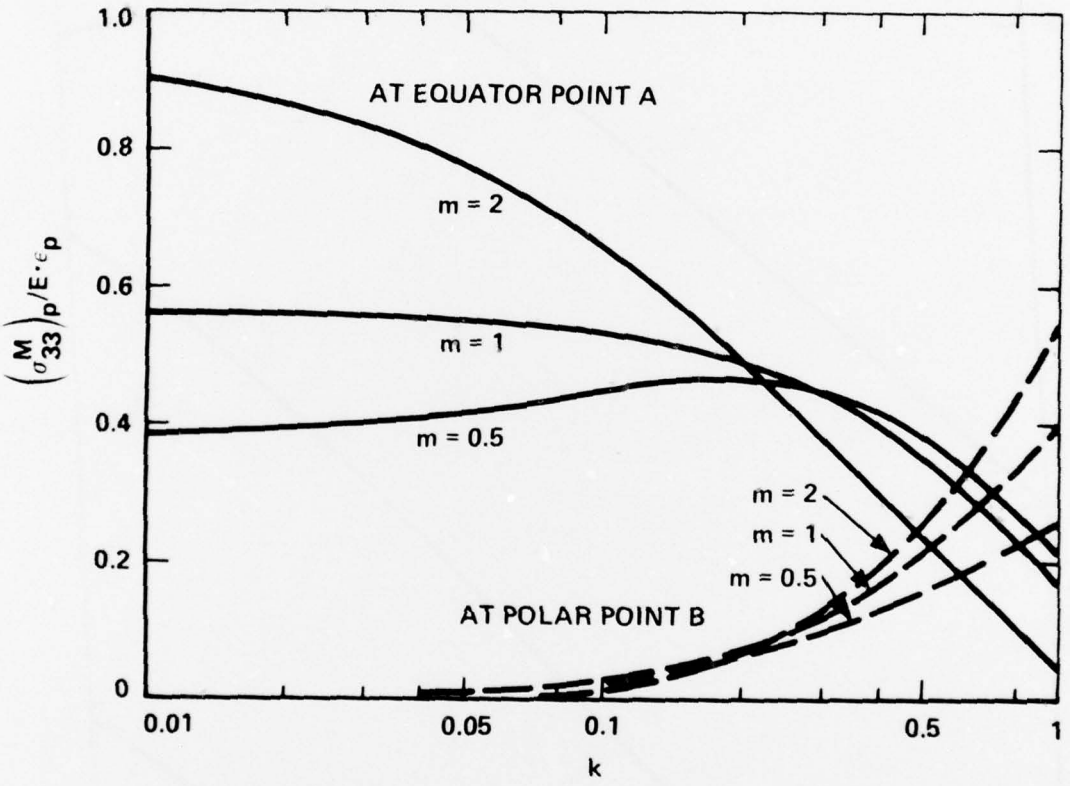

Fig. 13. Internal stress at equator point A and polar point B at the matrix-inclusion boundary due to plastic deformation effect. $\sigma^{M}_{33}/E\epsilon_p$ against k.

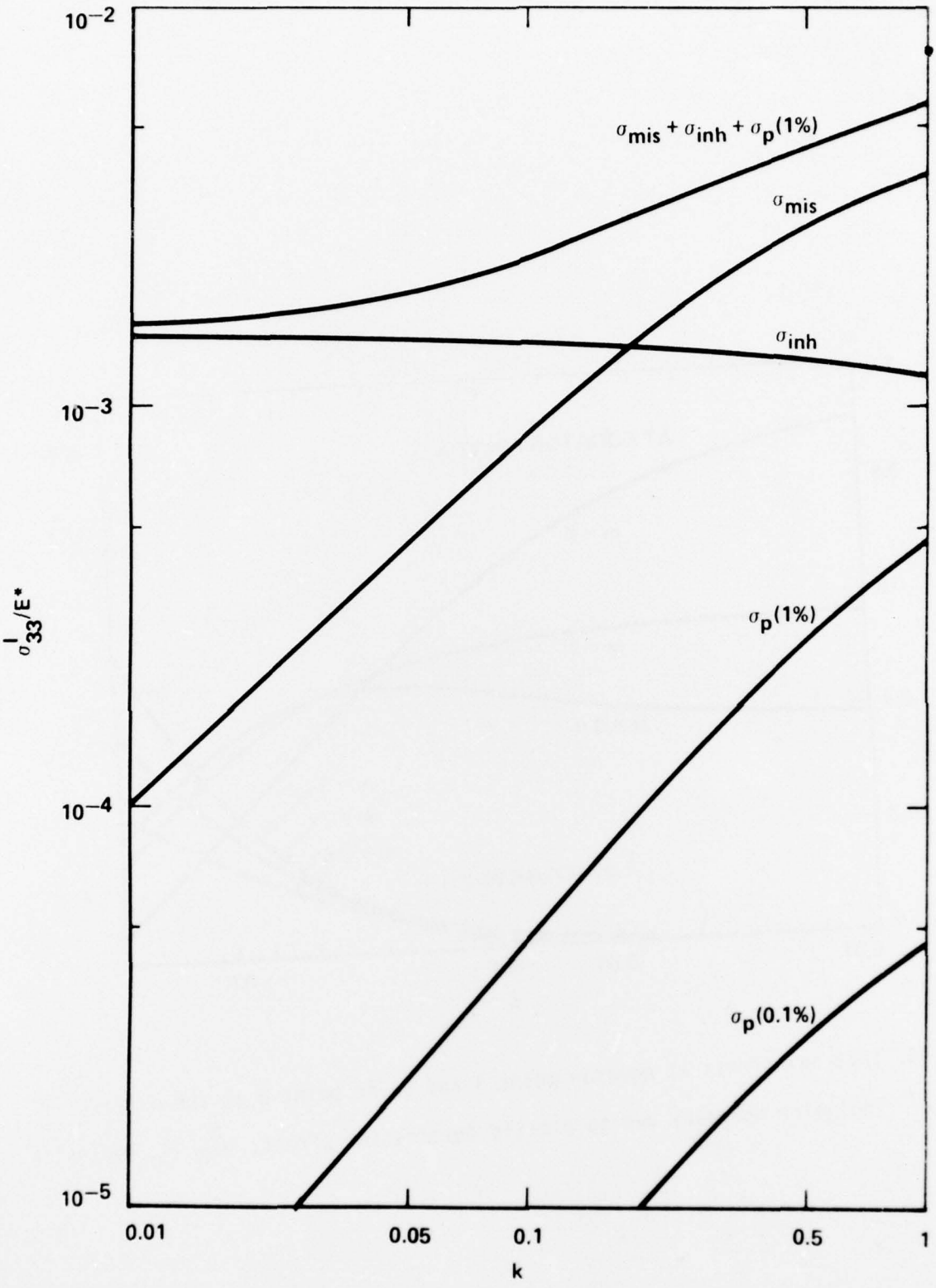

Fig. 14. Internal stress inside an oblate MnS inclusion in the steel matrix (m = 2/3). Three components of σ^I_{33} and their sum for the case of ε_p = 1% are shown against k. σ^A was taken as $10^{-3}E$ or $1.5 \times 10^{-3}E^*$.

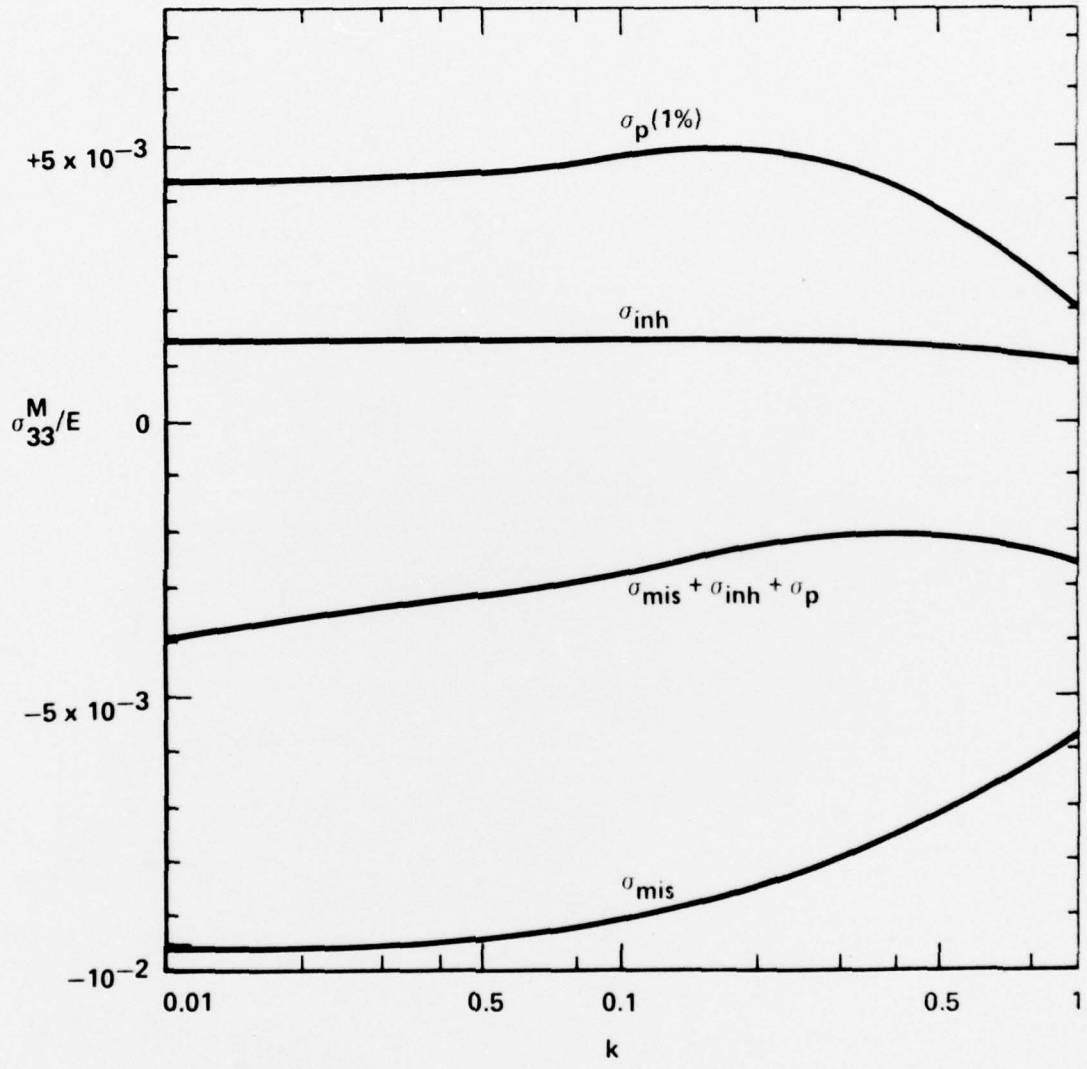

Fig. 15. Internal stress at equator point A of the matrix-inclusion boundary. σ^M_{33}/E against k. Note a large negative contribution due to misfit effect.